NTNU

Norwegian University of
Science and Technology

Sediment Erosion in Francis Turbines

Mette Eltvik

Master of Science in Engineering and ICT
Submission date: June 2009
Supervisor: Torbjørn Kristian Nielsen, EPT
Co-supervisor: Morten Kjeldsen, EPT
                         Ole Gunnar Dahlhaug, EPT
                         Per Egil Skåre, DynaVec AS

Norwegian University of Science and Technology
Department of Energy and Process Engineering

Problem Description

Sediment erosion in Francis turbines is a problem in areas with high concentration of sediments in the rivers. Near the Andes and the Himmalayas the rivers contains large amount of the hard and sharp mineral, quartz, which is damaging to the turbine components. During the monsoon period, the sand concentration is at its highest and maintenance intervals decrease rapidly. At Cahua power plant in Peru, the turbine components need to be changed annually since as much as 50kg/s of sediments passes through the turbines. Together with SN Power, Dynavec has developed a protected turbine with chemical coating, which desirable will reduce the number of maintenance intervals.

The aim of the master thesis is to predicting sediment erosion in Francis turbines. This is investigated by a CFD analysis of the stay, guide and runner vanes. Sand particles are implemented in the simulations, and a numerical erosion model calculates the erosion areas and intensity on the turbine.

Assignment given: 19. January 2009
Supervisor: Torbjørn Kristian Nielsen, EPT

Norges teknisk-
naturvitenskapelige universitet
NTNU

Fakultet for ingeniørvitenskap og teknologi
Institutt for energi- og prosessteknikk

EPT-H-2009-23

MASTEROPPGAVE

for

Mette Eltvik

Våren 2009

Sanderosjon i Francis Turbiner
Sediment Ersion in Francis Turbines

Bakgrunn

Sanderosjon i Francis turbiner er et problem i områder der det er mosunperioder i verden. Dette gjelder særlig for Himalaya og Andes der det i tillegg er store mengder med kvarts i sedimentene. SN-Power har inverstert i flere kraftverk i Peru som er meget belastet med sedimenter i monsun perioden. Ved Cahua Krafttverk så er det to Francis turbiner som har en effekt på 44 MW til sammen. I disse turbinene så går det i ekstreme perioder opp til 50 kg/s med sedimenter gjennom hver av disse turbinene. Dette medfører at de må bytte ut deler av turbinen hvert eneste år. SN-Power ønsker å forsterke turbinene slik at de kan ha færre vedlikeholdsintervall ved å legge på keramiske belegg på deler av turbinene.

Mål

Det er ønskelig å vite hvor i Francis turbinen sedimentene eroderer mest og hvorfor. Studenten vil gjennomføre CFD-analyse av turbinen. Denne CFD-analysen vil introdusere sediment partikkler slik at det er mulig å se hvor disse strømmer gjennom turbinen. Dette vil gi en forklaring på hvor sedimentene vil erodere mest i Francis turbine ved Cahua Kraftverk.

Oppgaven bearbeides ut fra følgende punkter:

1. Studenten må gjennomføre literatursøk for å se hva seom er state of the art innefor CFD-analyser med væske og faste partikkler sammen.
2. Studenten skal fortsette på arbeidet fra prosjektet med å gjennomføre CFD-analyser av stag skovler, ledeapparat og løpehjul på Cahua Kraftverk. Dersom det er tid skal også spiraltrommen introduseres i CFD-analysen.
3. Introdusere partikkler i CFD-analysen av ledeapparat og løpehjul på Cahua Kraftverk
4. Det skal etableres en sammenheng mellom CFD-analysene og teoretiske modeller for erosjon på metalliske overflater.

---- " ---

Senest 14 dager etter utlevering av oppgaven skal kandidaten levere/sende instituttet en detaljert fremdrift- og evt. forsøksplan for oppgaven til evaluering og evt. diskusjon med faglig ansvarlig/ veiledere. Detaljer ved evt. utførelse av dataprogrammer skal avtales nærmere i samråd med faglig ansvarlig.

Besvarelsen redigeres mest mulig som en forskningsrapport med et sammendrag både på norsk og engelsk, konklusjon, litteraturliste, innholdsfortegnelse etc. Ved utarbeidelsen av teksten skal kandidaten legge vekt på å gjøre teksten oversiktlig og velskrevet. Med henblikk på lesning av besvarelsen er det viktig at de nødvendige henvisninger for korresponderende steder i tekst, tabeller og figurer anføres på begge steder. Ved bedømmelsen legges det stor vekt på at resultatene er grundig bearbeidet, at de oppstilles tabellarisk og/eller grafisk på en oversiktlig måte, og at de er diskutert utførlig.

Alle benyttede kilder, også muntlige opplysninger, skal oppgis på fullstendig måte. (For tidsskrifter og bøker oppgis forfatter, tittel, årgang, sidetall og evt. figurnummer.)

Det forutsettes at kandidaten tar initiativ til og holder nødvendig kontakt med faglærer og veileder(e). Kandidaten skal rette seg etter de reglementer og retningslinjer som gjelder ved alle fagmiljøer som kandidaten har kontakt med gjennom sin utførelse av oppgaven, samt etter eventuelle pålegg fra Institutt for energi- og prosessteknikk.
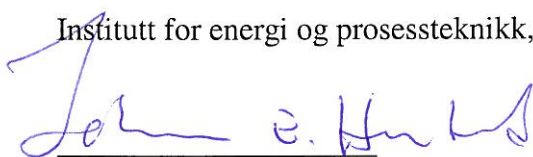
I henhold til "Utfyllende regler til studieforskriften for teknologistudiet/sivilingeniørstudiet" ved NTNU § 20, forbeholder instituttet seg retten til å benytte alle resultater i undervisnings- og forskningsformål, samt til publikasjoner.

Ett -1 komplett eksemplar av originalbesvarelsen av oppgaven skal innleveres til samme adressat som den ble utlevert fra. (Det skal medfølge et konsentrert sammendrag på maks. en maskinskrevet side med dobbel linjeavstand med forfatternavn og oppgavetittel for evt. referering i tidsskrifter).
Til Instituttet innleveres to - 2 komplette, kopier av besvarelsen. Ytterligere kopier til evt. medveiledere/oppgavegivere skal avtales med, og evt. leveres direkte til, de respektive.
Til instituttet innleveres også en komplett kopi (inkl. konsentrerte sammendrag) på CD-ROM i Word-format eller tilsvarende.

Institutt for energi og prosessteknikk, 12. januar 2009

Johan E. Hustad
Instituttleder

Torbjørn Nielsen
Faglærer/veileder

Medveiledere: Morten Kjeldsen
                  Ole G Dahlhaug
                  Per Egil Skåre   DynaVec AS

Preface

This master thesis was written at the Water Power Laboratory, Department of Energy and Process Engineering at Norwegian University of Science and Technology (NTNU) spring 2009. This work is a continuation of a project assignment of the author, finished autumn 2008. The thesis is an collaboration between SN Power and Dynavec.

The aim of the master thesis is to compare and verify CFD-simulations of sand erosion in Francis turbines with experiments and theoretical models.

I would like to thank my supervisors Ole Gunnar Dahlhaug and Torbjørn Nielsen for their support. Thanks to Ola Gjølme Thorvaldsen at Dynavec for help and advies, and to PhD student Hari Neopane at NTNU for collaboration during the thesis. A great thanks to Tore Castberg at HiST (College in South Trøndelag) for contribution and discussions. A special thanks to my fellow students for making a great working environment at the Water Power Laboratory.

Trondheim, June 10, 2009

Mette Eltvik

Mette Eltvik

II

Summary

The high concentration of sediments in the rivers near the Andes and the Himmalayas, is a large problems for run-of-river power plants. Small particles of quartz, which is a hard and sharp mineral, damage the turbine and causes reduced performance, shut downs of power plants and often extensive repairs. At Cahua power plant in Peru, turbine components need to be changed annually since as much as 50 kg/s of sediments passes through the turbines. Together with SN Power, Dynavec have installed a bolted turbine with a chemical coating, which desirable will reduce the maintenance interval.

This master thesis has the objective of predicting sediment erosion in Francis turbines. By the use of CFD analysis of the stay, guide and runner vanes, the erosion areas and intensity can be found. This is investigated by implementing particles in the numerical simulations and utilizing Langrangian particle tracking to predict the particles path through the turbine. With a numerical erosion model, the erosion areas and degree of intensity can be determined.

Results show that the numerical simulations give reasonably prediction of erosion trends. Vulnerable areas are detected at the upper and lower covers and runner blade surfaces, which agrees with the observations at Cahua power plant. A comparison between the numerical and theoretical models for erosion on material is made with a verification model. The model is a high velocity jet test rig which test sediment influence on materials. The simulations indicate similar erosion trends, however, the erosion intensity rate does not agree with results from experiments.

Sediment erosion is a highly complicated phenomena, and is dependent upon several factors. Numerical erosion models, will, with some modifications, give a good prediction of erosion areas and relative values of the erosion intensity. The simulations can be utilized to predict the location of severe erosion and to estimate maintenance intervals.

IV

Sammendrag

I elvene ved Andes fjellene og Himmalaia er konsentrasjonen av sedimenter høy, noe som er et stort problem for elvekraftverk. Turbinene er særlig utsatt for små partikler av kvarts, som er et hardt og skarpt mineral. Dette forårsaker redusert ytelse, hyppige reparasjoner og stengning av anlegg. På Cahua kraftstasjon i Peru, passerer så mye som 50 kg/s sedimenter gjennom turbinen slik at de må byttes ut årlig. I samarbeid med SN Power, har Dynavaec installert en boltet Francis turbin. Hele turbinen har et keramisk belegg for beskyttelse mot sand erosjon. Disse tiltakene er gjort for å kunne øke produksjonen og levetiden.

Målet med denne hovedoppgaven er å forutse sanderosjon på Francisturbiner. Ved bruk av CFD - analyser av stagskovler, ledeapparat og løpehjul, kan man finne potensielle erosjonsområder, og tilhørende intensitet. Ved bruk av Langrangian Particle Tracking - modellen kan partikler implementeres i den numeriske simuleringen og partikkelbanene igjennom turbinen beregnes. Numeriske erosjonsmodeller kalkulerer områder og omfagnet av erosjonsskaden i turbinen.

Resultatene viser at numeriske simuleringer gir en akseptabel forutsigelse av erosjonstendensen i turbinen. Som observert på Cahua kraftstasjon er de mest utsatte områdene øvre og nedre lokk og overflaten på løpehjulsskovlene. En verifiseringsmodell er laget for å kunne sammenligne numeriske og teoretiske erosjonsmodeller for metalliske overflater. Modellen er en rigg med en høyhastighest dyse som tester sanderosjon på ulike materialer. Simuleringene indikerer liknende erosjonstendens, men erosjonsintensiteten stemmer ikke overens med resultater fra eksperimenter.

Erosjonsproblem er et komplisert fenomen og avhengig av flere faktorer. Numeriske modeller med modifikasjoner vil kunne forutse erosjonsområder og gi relative verdier for erosjonsintensiteten. Simuleringene kan brukes til å lokalisere utsatte erosjonsområder, optimalisere design og estimerer vedlikeholdsintervaller.

Contents

List of Figures

List of Tables

Nomenclature

Symbol	Description	Unit
A	Cross section	m^3
C	Force coefficient	-
d	diameter	m
g	Gravitational acceleration	m/s^2
F	Force	N
K	Constant	-
k	Tabakoffs empirical constant	-
M	Dimensionless mass	-
m	Mass	kg
$\dot{N}$	Particle number rate	-
n	Exponent value for velocity	-
r	Radius	m
t	Time	s
U	Velocity	m/s
W	Erosion wear	kg/kg
W_c	Cutting wear	kg/kg
W_d	Deformation wear	kg/kg
X	Flux variable	-
Δx	Cell sixe in x-direction	-

Greek symbols

α	Impact angle	°
ϵ	Concentration rate	-
ρ	Density	kg/m^3
γ	Impact angle in radians	rad
ω	Angular velocity	$\frac{1}{s}$ r/min

Subscript

0   Reference value
B   Buoyancy
D   Drag
f   Fluid
fl   Fluctuation
i Calculation point
L   Lift
m   Material
P   Pressure
p   Particle
R   Rotational
VM   Added mass

Abbreviations

BEP   Best Efficiency Point
CFD   Computational Fluid Dynamics
HiST   College in South Trøndelag
NTNU   The Norwegian University of Science and Technology
PPM   Parts Per Million
SN Power   Statkarft Norfund Power Invest

Chapter 1

Introduction

1.1 Background

The power demand increases worldwide and due to the climate changes, the focus on green energy has increased. Among the different energy sources, hydro power is an economical, environment friendly and low-polluting source. Countries neighbouring mountain ranges like Himalayas and Andes mountain, have an interest to develop the hydro power potential, but the monsoon periods are challenging. Especially small and mini hydro power plants, with run-of-river schemes, have one major problem; the high sediment concentration in the river.

In Peru, the monsoon period lasts from November to April and the sediment concentration increases drastically. In the river near Cahua power plant, Rio Pativilca, 33% of the minerals is very hard and sharp quartz, and during the monsoon period the sediment concentration may be up to 25 000PPM[8]. The turbine parts are therefore especially vulnerable for erosion wear, and turbine parts needs overhauling every year. Worn out turbines leads to blade alteration, vibrations problems, reduces performance and efficiency, shut down of power plants and costly reparations. Together with SN Power, Dynavec AS has invented a bolted turbine with replaceable blades, coated with Wolfram carbide. The turbine is now installed at Cahua power plant in Peru. This setup is believed to be able to resist the erosion wear in a much better way than a conventional construction.

1.2 Objective

This thesis proceeds on the author's project assignment dealing with sediment erosion in Francis turbines. Simulations with Ansys CFX, which is a Computational Fluid Dynamic (CFD) software, can be utilized to predict potential erosion areas in the turbine. The aim

of this master thesis is to continue with the CFD-simulation and make a relation between the results from the numerical simulations and theoretical models.

1.3 Outline

The assignment begins with background information about the power situation in South America. As basic theory about sediment erosion and CFD theory is covered by the authors project[11], some chapters from the report are attached in the appendix. Supplementary theory about these topics is given in chapter 3, 4 and 5. Chapter 6 is about a verification model to confirm that the CFD model is applicable. Set-up of the CFD model of the Francis turbine is given in chapter 7. Further follows the results, discussion and conclusion.

1.4 Comments

In April, the author visited the Cahua power plant in Peru. Both units were shut down and it was possible to inspect the spiral case, stay vanes, guide vanes and the runner. Comparison between the numerical simulations and the real turbines is included in this report.

Chapter 2

Background

2.1 Sediment problems in South America

The Andes mountains ranges from Colombia to Chile and is the worlds longest mountain range with its 9000km. Rain, wind, snow and glaciers erodes the mountains, and fragments of minerals and rock breaks off. Water in motion transport the sediments down the river. The common problem for many of these run-of-river power plants is the high concentration of sediments in the river. Even with settling basins, the concentration of small sediments in the water is high. Quartz is a common mineral in the Andes mountains, and this mineral is damaging for the turbines due to its hardness.

In Peru, SN Power has eight hydro power centres with a total installed capacity of 280MW. The marked is competitive with many strong players, both existing and new. Peru's economy is strong and seems to continue to growing the next years. Earlier the Peruvians have suffered from political disturbance, but the president Garcia has pursued a policy friendly to foreign investors. Investment in new hydro power plants will give a good opportunity for development projects in the future. In Chile, the potential of hydro power is 24 000 MW, but SN Power has only utilized 4050 MW today. Earlier, Argentina supplied Chile with gas, but this transfer suddenly stopped due to energy problem in Argentina, they need the gas for themselves. Chile got an energy shortage, but decided to build up an energy system of their own. The aim is to have an independent energy production.

The potential of hydro power in Brazil is large, only Canada has a larger production of hydro power. Due to a political stability, economic growth and an increasing power demand of 4 000 MW p.a., it is a good marked. The most important energy source in Colombia is hydro power, which represented 67% of the total effective capacity. For larger plants, 100 MW, the potential is 85 TW. In over 40 years Colombia has suffered from armed conflicts, but in the last five years, the politic and economy situation seems to be stabilized[12].

Another problem is the treatment of the native people and their land. They have been

resisting constructions of dams and power plants. Many of the existing and planed power plants is of run-of-river types, which means that the local geography will not be affected in the same degree as with a big reservoir.

The power plant managers want to produce as much energy as feasible and a high efficiency is important.In areas like the Andes, only after few months or years the turbine performance will decrease due to the sediment problems. Frequently shut-down of power plants is necessary to rehabilitate turbine parts, the energy production decreases and the profit is lost. Thus a solution to the sediment problem is a very important task in these countries.

Chapter 3

Sediment Erosion Theory

The rate of erosion depends on particle properties(size, shape, hardness, concentration), erosion mechanism (cutting, deformation) and fluid characteristics (velocities, turbulence) In Appendix A, the chapter from the project thesis about basic sediment erosion theory is included. This chapter will contain supplementary theory about sediment erosion.

3.1   Erosion mechanism

Sand erosion appear as micro abrasive pitting and gradually take shape as fish shell or wave shaped grooves. When the particles collides with the surface, the kinetic energy is converted to work, which gives deformation of the material. Duan and Karelin[10] classified erosion wear into two basic mechanisms. The main factors that affects the erosion are the impact angle and particle velocity as seen in figure 3.1:
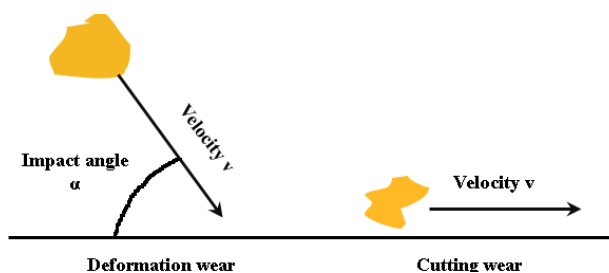

Figure 3.1: Erosion mechanism

The *cutting wear*, or abrasive erosion, is due to particles with low impact angles, rolling or sliding along the surface, and material is removed due to scratching or cutting in the surface. Erosion intensity depends mainly upon velocity and impact angle, but also particle shape

and hardness matters. Particles with sharp edges will leave a long scar in the material. *Deformation wear* is when the surface is exposed to continuous collision of particles with a large impact angle. Due to material fatigue, plastic deformations takes place and the surface gradually get harder and more brittle and parts of the material are removed.

These two mechanisms can be divided into four mechanical effects which is relevant for erosion wear in hydraulic machinery[17]:

Abrasive erosion
Abrasive erosion is understood as microscopic surface tearing of material. The particles slides over the surface with a low impact angle. Due to sharp edge on the particles, material is removed.

Brittle fracture
A brittle fracture occurs as a result of particles with high impact angle and medium velocity hits the surface. Cracks develops and fragmentation of material can be an effect.

Plastic deformation
Flake formation is another results of strikes from particles with high impact angle and medium velocity. Plastic deformation occurs and debris of materials breaks off.

Fatigue of surface
Particles with high impact angle and low speed will strike the surface and makes the material poor. Continuous hitting of particles trigger cracks to appear in the surface and due to fatigue, material will be detached.

3.2 Sand properties

The erosion rate is highly dependent on the properties of the particles. In appendix A these properties are described. A brief overview is given here[3, 6]:

- Shape and size - Sharp edged particles cause more erosion than round shaped. Large particles(>0.25mm) gives greater damage than small particles.

- Hardness - According to Moh's hardness scale, particles with value above 5 will be harmful. The erosion intensity is proportional to the hardness of the particle.

- Concentration - Defined as mass of particle present in the unit mass, PPM (parts per million). This factor has the largest influence on the erosion intensity - Erosion rate is linearly proportional to the concentration of particles.

In figure 3.2, the erosion rate versus impact angle for brittle and ductile materials is given by mass of material removed per unit mass of particles. For low impact angles and sharp particles, the ductile material is most vulnerable for abrasive erosion. The erosion rate decreases with impact angles higher than 25°, and then the wear results in deformation
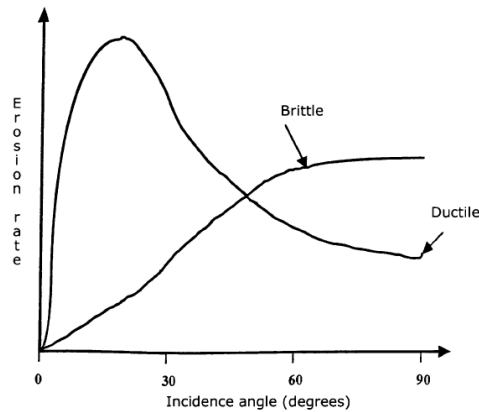
Figure 3.2: Erosion rate at different impact angle for ductile and brittle materials[14]

of the material rather than erosion. Brittle material is more exposed to larger impact angles, were crack formations in the surface is due to plastic deformation and also partly to fatigue in the material. For angles laying in between, both cutting and deformation erosion contributes and gives medium erosion rate[17].

3.2.1 Forces acting on the particles

The fluid flow influence the particles velocity and direction, and several forces are acting on the particles on their path through the turbine. The particles will by affected of two different force categories[3, 9]:

- Stabilizing forces - Viscous and gravity forces retard movements of the particles and have a stabilizing effect.

- Destabilizing forces - Due to centrifugal and Coriolis forces the sediment will slide along the bed with a low velocity, called bed-load. The turbulence forces will cause irregular movements in the fluid and thereby also of the particles, as they move in the same direction as the fluid surrounding them.

Lift and drag forces
The drag force works in the direction of the main flow, and the lift force in the transverse direction. The forces are proportional to the square of the flow velocity:

$$F_D = \frac{1}{2}C_D A_p \rho U^2 \quad F_L = C_L A_p \rho_f U^2 \tag{3.1}$$
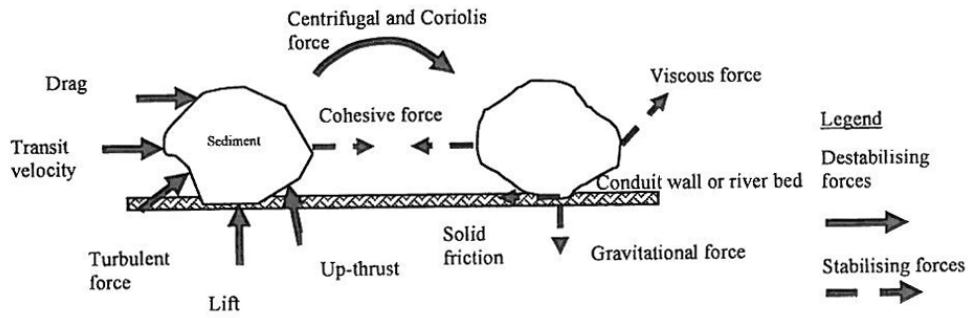
Figure 3.3: Forces acting on the particles

where

A_p	Particle cross section
C_D	Drag force coefficient
C_L	Lift force coefficient
F_D	Drag force
F_L	Lift force
U	Velocity
ρ_f	Fluid density

The buoyancy force

The buoyancy force is an effect of the difference between the density of the fluid and particles. The gravity effect influences the particle motion.

$$F_B = \frac{\pi}{6} d_p^3 (\rho_p - \rho_F) g \tag{3.2}$$

where

F_B	Buoyancy force
d_p	Particle diameter
ρ_f	Fluid density
ρ_p	Particle density
g	Gravitational acceleration

Rotation force

The sum of Coriolis and centripetal forces are the rotation forces acting in a rotating domain.

$$F_R = m(-2\omega \times U_p - \omega \times \omega \times r_p) \tag{3.3}$$

where

F_R	Rotation force
m	Mass
r_p	Particle radius
U_p	Particle velocity
ω	Rotational speed

Turbulence force
Eddies are formed in an irregular flow due to shearing action inside the flow. Eddies will form and dissipate irregularly, and this disorderly flow is what is called turbulence effect.

3.3 Erosion models

A theoretical estimation of erosion intensity depends upon several variables. It is difficult to define these variables with exact mathematical accuracy, and for the present, an accurate mathematical model is not found. Erosion in hydraulic machinery is complicated due to complex relations between different factors like turbine design, operating conditions, fluid and sediment properties. Research work utilize field experiments to develop empirical and statistical relations. The use of numerical modelling and simulations have become an important tool to achieve more knowledge about erosion wear.

Bitters erosion model [10] defines erosion wear as described in the beginning of this chapter. The amount of wear W equal to the sum of cutting wear, W_c, and deformation wear, W_d, defined by the following equations:

$$W = W_d + W_c \tag{3.4}$$

$$W_d = \frac{\frac{1}{2}\rho_m(U_p\sin\alpha - K_3)}{C_3} \tag{3.5}$$

$$W_c = \begin{cases} \frac{\rho_m C_1 U_p^2}{K_2}[\sin 2\alpha - \frac{K_1}{C_2}\sin^2\alpha] & \text{for } \tan\alpha < \frac{C_2}{K_1} \\ \frac{\rho_m C_2 U_p^2}{K_2}[\frac{C_2}{K_1}\cos^2\alpha] & \text{for } \tan\alpha > \frac{C_2}{K_1} \end{cases} \tag{3.6}$$

where
$C_1 C_2 C_3$	Empirical constants
$K_1 K_2$	Empirical constants
U_p	Particle velocity
W	Erosion wear
W_c	Cutting wear
W_d	Deformation wear
α	Impact angle
ρ_m	Material density

Only a few erosion models is specified for hydraulic machinery. Most of the models are made for specific conditions, such as Bitter's model which is based on observations of cast iron particles hitting a silver plate.

Duan et al.[10] gave a theoretical evaluation of abrasion intensity which, compared to experiments, gives good accuracy. The mathematical relation of erosion on a blade surface

considers a stationary plate with an uniform steady fluid stream normal to the surface.

$$W = K m_p \epsilon U^3 t \qquad (3.7)$$

where
K	Constant
m_p	Particle mass
U_p	Particle velocity
t	Time
W	Erosion wear
ϵ	Concentration rate

A theoretical model for silt erosion on turbine parts is given in IEC 62364(rev.7)[15]. The formula is simplified to be suitable for hydraulic machineries, and the constants can be adjusted for all the turbine components. The model is given by:

$$W = K \cdot K_m \cdot K_{flow} \cdot K_{size} \cdot K_{shape} \cdot K_{hardness} \cdot \epsilon \cdot U_p^n \qquad (3.8)$$

where
W	Erosion wear
K	Constant
K_{flow}	Flow constant
$K_{hardness}$	Hardness constant
K_m	Material constant
K_{size}	Particle size constant
K_{shape}	Particle shape constant
ϵ	Concentration rate
U_p	Particle Velocity
n	Exponent value

The erosion rate, W, is the loss of thickness per unit time. Thus some assumptions need to be clarified:

- The relative particle velocity,U, will be considered constant over time.
- Flow pattern, physical properties for particles and material do not vary over time
- Concentration of particles, ϵ, will be integrated over time and is defined as $[\frac{kg \cdot hr}{m^3}]$:

$$Concentration = \int_0^t \epsilon(t) dt \qquad (3.9)$$

The exponent in the velocity factor, U^n, can be a value between 2 and 5, but IEC recommend to use 3. Particle size, K_{size} and particle shape, K_{shape}, is set to 1. $K_{hardness}$ is the relation between hardness of particle and turbine material(not valid for coated components). The flow pattern, K_flow, has to be defined for every component. The material properties for the turbine, K_m, depends on the material: 1 for stainless steel 13Cr4Ni, 2 for carbon steel, and less then 1 for coated components, depending on the coating material.

Chapter 4

Sediment Erosion in Francis Turbines

Earlier, the turbines were more massive and rarely needed maintenance. Today the turbines are hydraulically optimized resulting in thinner blades and are thus more vulnerable to erosion. This chapter describes the erosion areas in Francis turbines based on experiments. The condition of the runners at Cahua power plant at the time of inspection is given.

4.1   Operating condition

Erosion rate is often said to be proportional to concentration, which is logical as the possibility that more particles will collide with the surface increases when the concentration increases. Many experiments is worked out, both in air and in water tanks. Some experiments show that the erosion increases with the flux rate to a specific limit, and then decrease due to interaction between particles. Other laboratory experiments indicate that erosion rate will be constant for higher flux rates, or no significant erosion is detected. The experiments indicates that the correlation between concentration and erosion rate is highly dependent upon materials, synergy effect between erosion and corrosion, impact angles and test equipment[10, 17].

In a Francis turbine the flow situation is different, and the erosion rate will be a highly affected by the operation of the turbine. Operation at off design causes a higher erosion rate due to the increased turbulence, and secondary flows and vortices are likely to occur. Especially the guide vanes and runner are exposed to greater wear during operations at full load. Often start and shutdown of the power plant is detrimental to the turbine components. This will cause oscillations in the water conduit and bring sediments from the tunnels and channels through the turbine.

4.2 Sand erosion categories

Duan et al.[10] classified sand erosion into three categories:

- *Turbulence erosion* - Due to high turbulence in the boundary layers, the small particles will get a significant rotational velocity and induce strong abrasive erosion on the surfaces.

- *Acceleration* - Particles can be separated from the flow due to accelerations normal to the stream lines, and collide with the walls.

- *Secondary flow vortex erosion* is found in vortices around corners, in a horse shoe vortex or areas were the high velocity and accelerated flow cause vortices and secondary flow.

The most critical areas exposed to sediment erosion are those where high velocities and/or high accelerations occur. A classification of sediment erosion is essential when describing erosion damage on the turbine[10].

1. Metallic lustre - A shining surface with no traces of paint, scale or rust.

2. Fine-scaly erosion - A surface with rare, separately located and skin-deep scales.

3. Scaly erosion - A surface entirely covered with skin-deep fine scales.

4. Large-sized scaly erosion - A surface entirely covered with deep and enlarged scales.

5. In-depth erosion - A surface covered with deep and long channels.

6. Through holes or entire metal wear out.

4.3 Erosion areas

(a) Inlet of the stay vanes

(b) Typical ring-grooves near the stay vane leading edge

Figure 4.1: Erosion on stay vanes at Cahua power plant

4.3.1 Stay Vane

The purpose of the stay vanes is to hold the spiral case together, and direct the flow direction into the turbine. In the spiral case, secondary flow occurs and causes an incorrect flow angle towards the stay vane inlets. Paint and material is removed due to turbulence erosion at the upper and lower area of the stay vane inlet, marked with red in figure 4.1. The mid height of the leading edge part is exposed to less erosion intensity. Near the upper and lower cover at the inlet, ring-shaped erosion grooves can be observed, see figure 4.1 b.

4.3.2 Guide Vane

Wear at the guide vanes is generally scaly erosion of different intensity levels, from grade 2 to 4, see figure 4.2. The greatest erosion is observed near the transitional zone to the lower cover, due to the high acceleration and absolute velocity in the guide vane cascade. Also at the outlet region near the trailing edge severe erosion occurs. This is so because absolute velocity is at the highest here,and turbulent erosion increases.

Figure 4.2: Eroded guide vanes, Cahua power plant

The covers will be exposed to erosion since the acceleration normal to the streamline creates secondary flow. Especially at the corners between the facing plates and guide vane as seen in figure 4.3. This effect occur because of the horse shoe vortex and heavy erosion grooves is observed. At the stagnation point in the guide vane inlet, a horse shoe vortex occurs and follows along the blades adjacent to the covers. In the clearance between the guide vane and the facing plates, a leakage flow passes and creates erosion. On the suction side of the vane the horse shoe vortex will increase as a consequence of the cross flow leakage. Leakage erosion will also induce local separations and turbulence which will produce heavy erosion at the inlet pressure side and the outlet section. The main flow is accelerating through the guide vane channel, thus the water in front of the runner rotates and creates a secondary flow. Acceleration of particles normal to the streamline therefore induces erosion areas around the corners at hub and shroud.

Figure 4.3: Horse shoe vortex of facing plates in the guide vane channel, Cahua power plant

4.3.3 Runner vane

The highest acceleration in the turbine takes place at the blade inlet, and the highest relative velocities at the outlet. As seen in figure 4.4, deep grooves occurs at the inlet blade roots. At off-design operations, the local accelerations will be higher and secondary flow erosion will occur. A horse shoe vortex occurs due to the incorrect blade leaning, and deep erosion grooves is observed near the blade roots. The inlet is also vulnerable for incorrect pressure distribution due to large pressure gradients between the pressure and suction side.

At the surface of the blade, abrasive erosion is present at the pressure side, intensifying in the direction of the trailing edge. Turbulence erosion takes place near the outlet area due to increasing relative velocities. The trailing edge near the shroud is subjected to both sediment erosion and cavitation erosion. Low pressure areas can lead to cavitation, which amplify the erosion on the runner outlet. The combination of abrasive and cavitation erosion tears the material and the thickness of the edge will decrease. This is what is called cavitation erosion, which is crucial to the turbine. The outcome of these two effects, is deterioration of material and that knife-sharp jag becomes visible, see figure 4.5.

In the stream line direction, the hub is subjected to a growing rate of erosion. Starting at the leading edge with fine-scaly erosion (grade 2) and increasing to large-sized scaly erosion (grade 4) closer to the trailing edge. This is due to streamline acceleration along the blade. Higher erosion rate is found at the shroud, especially near the leading and trailing edge, marked as red in figure 4.5. In-depth erosion (grade 5), starting from the leading edge to the outlet, is due to cavitation erosion.

Figure 4.4: Old runner, Cahua power plant

Figure 4.5: Erosion at runner outlet, Cahua power plant

4.4 Inspection at Cahua power plant

In 2003, the Cahua power plant was purchased by SN Power. Cahua power plant is a run-of-river plant 260km north of Lima. Two vertical Francis turbines, each with a capacity of 22 MW, is installed. The mass flow rate is $10m^3/s$ and the gross head is 215 meter. The average annual output is 280GWh[13].

Since In March 2009, the coated turbine from Dynavec was installed. After only six weeks of operation and as much as 120 000 tons of sediment, the author visited Cahua power plant for a few inspection. Since installation in March, the coated Dynavec runner had been operating at full load, with stops only during inspections. Erosion was found at the trailing edge, in the area between the blade and shroud. This is the most critical erosion area. At the leading edge at the blade junction to the hub, erosion grooves could be seen. At the transition between blade, hub and shroud, the sediments had started to wear and to remove material under the coating layer. Thus, flakes of coating are broken off. These areas have typical secondary flow vortices and turbulence flow occurs at the blade root. The guide vanes surfaces had minor visible erosion. At the transition between the guide vane and the facing plates erosion tendency was observed, and especially near the lower cover, bad grooves were seen.

Concerning the other turbine, which had been in operation since May 2008, only 90 000 tons of sediments had passed through it during that time. This because the turbine was stopped whenever the sediment concentration exceeded 3000 PPM. Larger erosion areas at the inlet and outlet of the runner were detected. Fine-scaly erosion was seen at the hub surface. The shroud had in-depth erosion cuts which started at the leading edge and increases towards the trailing edge. Erosion at the tailing edge was very large and material was worn out, and a knife-like jag was similar for all the blades. The guide vanes had fine-scaly erosion on the surface, and leakage flow had made typical horse shoe marks at the covers.

Comparing these turbines, the coated runner was in good condition considering the amount of sediments that had passed trough it. The uncoated turbines was more damaged after even less amount of sediment passing trough it, as could be observed at the other runner, see figure 4.5.

Materials in hydraulic turbines
The most commons materials used in Francis turbines are the 13Cr4Ni and 16Cr5Ni stainless steels. They are both austenitic-martensitic steels with good weldability, ductility, impact resistant and fatigue resistant properties. Due to its resistance to corrosion and cavitation, the materials are suitable for hydraulic applications. The turbine from Dynavec is coated with wolfram carbide which is a dense and hard material with very good temperature and corrosion resistance properties[2].

Chapter 5

CFD theory

All simulations are accomplished with three-dimensional Navier Stokes solver Ansys CFX 11.0. For more background information about general CFD-theory the reader is recommended to read through Appendix B.

5.1   Grid properties

The grid plays an essential role in the CFD simulation and it is important to get familiar with the different grid options. The choice of properties will affect the accuracy and convergence of the solution. The partial differential equations, given in Appendix B, governs the physics in a fluid domain. When analysing the flow in the domain, the equations is discretized and solved for each node. In Ansys CFX the Finite Volume Method (FVM) is used to transform these equations to a set of algebraic equations. The first step is to divide the fluid domain into many small elements, called cells or control volumes. The network of all the control volumes in the domain is called a mesh or grid. Each control volume has a node were all the information of velocities, pressure, temperature i.e., is stored. The fluid characteristic is transferred from one node to the neighbour node, and the approximate solution for all elements gives a picture of the fluid flow in the domain.

5.2   Numerical model

To achieve a result with second order accuracy and sufficient numerical stability, the high resolution scheme is applied for discretization of the grid. The algebraic equations are solved iteratively with the MUSCL approach, which stands for Monotone Upstream centred

Scheme for Conservative Laws. The upstream method is based on the principle of choosing the flux from the upwind side. Equation 5.1 is the upstream difference in x-direction:

$$\frac{\partial X_i}{\partial x} = -\frac{X_{i+1} - X_i}{\Delta x_i} \tag{5.1}$$

X   Flux variable
δx Cell sixe in x-direction
i Calculation point

The difference between the values between the nodes upstream and downstream of i, is the derivative in point i. The MUSCL approach is second order accurate which means that the dispersion term is $O(\Delta x^2)$. The approximation gets better the smaller Δx is, thus the grid should be as fine as possible[3, 18].

5.2.1   Forces acting on the particles

Forces are acting on a particle moving in a continuous fluid. Differences between the fluid velocity and particle velocity will influence the acceleration of the particle. From Newtons second law the rate of change of velocity is calculated:

$$F = m_p \frac{dU_p}{dt} \tag{5.2}$$

F Resultant force
m_p Particle mass
U_p Particle velocity
t   Time

Basset et al.[3] derived the equation of motion for a particle in a rotating frame. The equation can be rewritten to:

$$F_D + F_B + F_R + F_{VM} + F_P = m_p \frac{dU_p}{dt} \tag{5.3}$$

F_D Drag force
F_B Buoyancy force
F_R Rotational force
F_{VM} Added mass force
F_p Pressuer force
m_p Particle mass
U_p Particle velocity
t   Time

F_D is the drag forces which is the major force affecting the particle flow. F_B is the buoyancy force due to gravity and is necessary when the density difference between fluid and particle is significant. The rotating forces, F_R, includes both centripetal and Coriolis forces and is very important for models with rotating frame of reference. The added mass force, F_{VM}, account for the inertia of the surrounding fluid. F_p is the pressure gradient acting on the particle. Due to acceleration the pressure gradient to the fluid will change and affect the movement of the particle.

Turbulent Dispersion Force
The fluid velocity is decomposed into two components, mean and fluctuating velocity[3]. The mean velocity component, $\bar{U}_f$, affects the average particle trajectory, and the fluctuating velocity component, u_f, causes dispersion of particles in a turbulent flow.

$$U_{fl} = \bar{U}_{fl} + u'_{fl} \tag{5.4}$$

U_{fl}	Fluctuation velocity
$\bar{U}_{fl}$	Mean velocity
u'_{fl}	Fluctuation velocity component

For small particles, this force is important to capture the dispersion of particles in the flow. The application of turbulent dispersion model resolves the interaction of a particle within a single turbulent eddy. As default, the Eddy Viscosity Ratio Limit is set to 5 in Ansys CFX. Only in areas where the turbulent viscosity ratio is above this limit, the turbulent dispersion force is activated. The fluctuation velocity for the eddy is added to the local mean fluid velocity when a particle is entering the eddy.

5.2.2   Turbulence models

The main problem with turbulence models is flow separation from smooth surfaces, and the standard two equation turbulence models, such as k-ϵ, often under-predict this phenomena. The k-ϵ model is considered as industry standard due to its stable and numerical robust calculations. In the near wall regions, a scalable wall-function is provided, see Appendix B. Limitations for the model are boundary layer separation, flows over curved surface and rotating fluids. A model which take care of these phenomena is the Shear-Stress-Transport model (SST). In the near wall region, the model uses an automatic near-wall function which switches between k-ϵ and k-ω depending on the distance to the wall. The model is more computational expensive than k-ϵ, but gives a better accuracy and is more robust[3].

5.3 Particle transport model

The overall mass flow rate of the particles is shared amongst the representative particles being tracked. By dividing by the (initial) mass of the particle, this means that each representative particle has a Particle Number Rate. This quantity is used internally in the code for calculating overall sources to the continuous phase, and is also used in post-processing for calculating mass flows of particles through boundaries, forces on walls, etc.

Langrangian particle tracking is the multiphase model used to calculate the particles trajectories through the turbine. The fluid contains a high concentration of quartz, but only a representative number of particles is calculated in the simulation to save computer performance. Each particle follows an individual path through the domains, representing a sample of particles. As the particles collide with the wall, the impingement information (velocity and location) is treated by a set of empirical erosion equations. These equations determines the material mass losses caused by the particle impact, and take into account the particle velocity, shape, impact angle, density and mechanical properties of the wall material. The method is most suitable for steady state analysis since each particle is tracked from a injection point to a final destination. The runner is a rotating part and Ansys CFX 11.0 has its limitations for particle tracking in moving domains. Transient simulations is therefore not possibility.

The simulations do not include these limitations:

- No particle-particle interaction or particle breakup

- Only spherical particles are considered

- The sliding effect of particles along the specimen is not possible to simulate.

- No geometry modification due to removed material.

5.4 Erosion model

To predict the erosion rate, two different models are available in Ansys CFX. *Finnie's erosion model* calculates the erosion rate in the simulation as:

$$W = \frac{U_p{}^n}{U_0} f(\gamma) \tag{5.5}$$

$$U_0 = \frac{1}{\sqrt[n]{K_m}} \tag{5.6}$$

W Erosion wear
U_p Particle velocity
U_0 Reference velocity
γ Impact angle in radians
n Exponent value for velocity
K_m Material constant

For metals, the exponents value, n, can be 2.3 to 2.5, but for Francis turbines the exponential value is recommended to be 3[?, Tri]

Another erosion model is available in Ansys CFX, *Tabakoff and Grant erosion model*, which take into account the erosion effect of quartz particles on stainless steel ST 304[14]. According to Tabkoff and Grant[3], the erosion rate is given by:

$$M = f(\gamma)(\frac{U_P^2}{U_1})^2 \cos^2\gamma[1 - R_T^2] + f(U_{PN}) \qquad (5.7)$$

M   Dimensionless mass
γ Impact angle in radians
U_p Particle velocity
$U_1, U_2\ U_PN$ Reference velocity

The empirical constants,k_1, k_{12} and γ_0, used in this erosion ratio equation is presented in table 5.1. The dependency of impact angle is given by:

$$f(\gamma) = [1 + k_2 k_{12}\sin(\gamma\frac{\pi/2}{\gamma_0})]^2 \qquad (5.8)$$

$$R_T = 1 - \frac{V_P}{V_3}sin\gamma \qquad (5.9)$$

$$f(V_{PN}) = (\frac{V_P}{V_2}sin\gamma)^4 \qquad (5.10)$$

$$U_1 = \frac{1}{\sqrt{k_{12}}} \qquad (5.11)$$

$$U_2 = \frac{1}{\sqrt[4]{k_2}} \qquad (5.12)$$

$$U_3 = \frac{1}{k_2} \qquad (5.13)$$

$$k_2 = \begin{cases} 1.0 & \text{if } \gamma \leq 2\gamma_0 \\ 0 & \text{if } \gamma \geq 2\gamma_0 \end{cases}$$

γ	Impact angle in radians
U_p	Particle velocity
U_1, U_2 $U_P N$	Reference velocity
k	Tabakoffs empirical constant

The total erosion rate is the sum of all the particles. The erosion wear in the simulations is defined as grams of eroded material per gram of colliding particles. The overall erosion rate is:

$$Erosion Rate = M \dot{N} m_p \qquad (5.14)$$

M	Dimensionless mass
$\dot{N}$	Particle number rate
m_p	Partcle mass

Variable	Value
Constant k_{12}	0.293328
Ref velocity V_1	123.72 [m/s]
Ref velocity V_2	352.99 [m/s]
Ref velocity V_3	179.29 [m/s]
Angle of maximum erosion γ_0	30 [deg]

Table 5.1: Coefficient for Tabakoff erosion model, quartz - 304 stainless steel

The values listed in table 5.1 are found after experiments with quartz particles on a stainless steel plate, type 304[17]. This type of steel is the most common type of stainless steel. Due to its high ductility, good corrosion and heat resisting, excellent drawing, forming and spinning properties the steel type is versatile[2].

Chapter 6

Verification model

In order to verify the CFD-model, a comparison between the numerical simulations and experiments was carried out in cooperation with Tore Castberg, a PhD-student at HiST (Sør-Trøndelag University College). The aim of the comparison is to look at the erosion areas for different velocities and angles. The experiments are performed by Castberg, at the high velocity erosion jet test rig in the erosion-corrosion laboratory at NTNU/SINTEF.
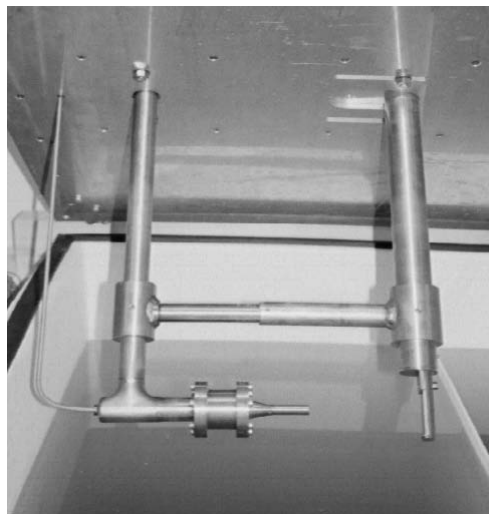

Figure 6.1: High velocity jet

6.1 Experimental overview

The high velocity erosion jet consists of a tank, nozzle, high pressure pump, water/sand blender, specimen holder and flow measuring device. The nozzle and specimen holder is

submerged in a fibreglass tank (1mx1mx2.4m) with total 1550 litres of water. Water is pumped through a nozzle with high velocity, and mixed with sand from a tube inside the nozzle. The mixture of water and sand particles will hit a specimen which is placed 102 mm from the nozzle exit, see figure 6.2. Dimensions for the specimen is 65x35mm, shown in figure 6.3. All the tests were consistent with three different water velocities (36, 60 and $74m/s$) and three angles on the specimen (45° 60° and 90°). The quartz size and concentration are held constant[7].
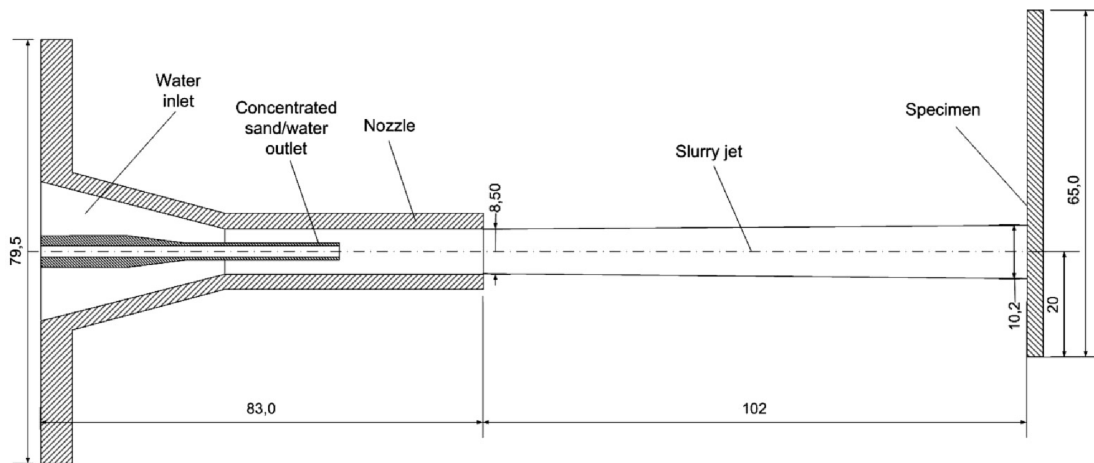
Figure 6.2: Jet dimensions
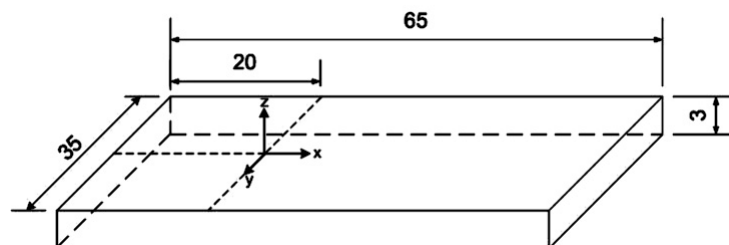
Figure 6.3: Specimen dimension

6.2 Numerical model

The sketching of the geometry, generation of the mesh and simulations were applied with Ansys Workbench. The boundary conditions for the simulations were specified in CFX-Pre, then solved in CFX-Solver and post processed in CFX-Post.

6.2.1   Geometry and mesh

A simplified geometry of the high velocity jet can be seen in figure 6.4. The geometry drawn extends from the inner nozzle, where the concentrated water and sand are mixed, to the specimen. Water leaves the nozzle at a specified velocity, hits the specimen and then sinks into the tank.
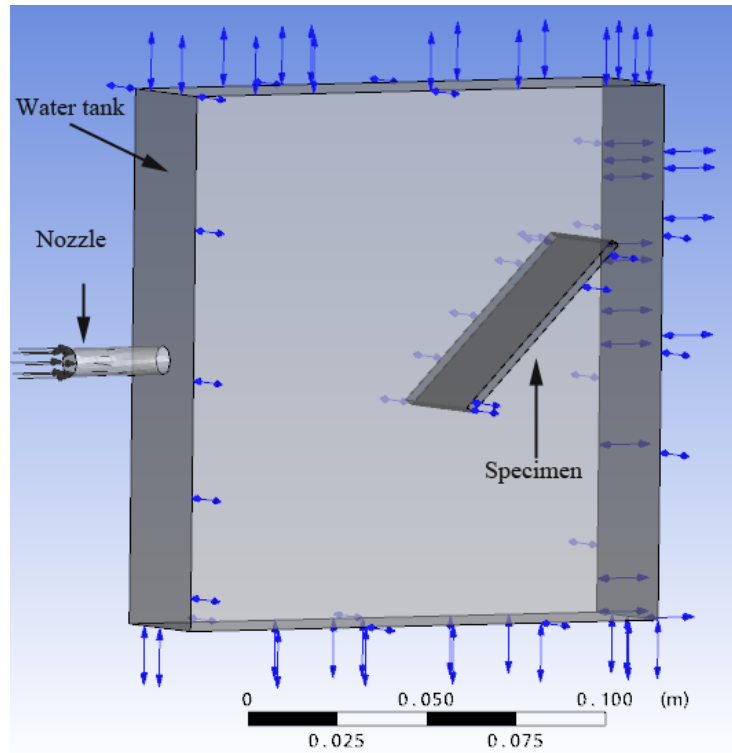
Figure 6.4: Geometry of model, 45°

The three different meshes are made for the particular angles, 45°60°and 90°, is generated in CFX-Mesh. At 90°, the particles hit normal to the specimen surface. The jet stream and specimen have the largest flow gradients and therefore have a refined grid. The surrounding areas have a course grid since the flow is less intense. In table 6.1 the total number of nodes for each mesh is presented:

Angle	Number of nodes
45°	147 163
60°	125 704
90°	170 835

Table 6.1: Mesh data

6.2.2   Boundary conditions

Steady state analysis of the 3D model was simulated with a k-ϵ turbulence model. The k-ϵ is a stable and numerical robust, two equations turbulence model, suitable for this simulation. Lagrangian particle tracking model was used to calculate the particle behaviour in the domain. The simulation calculates quartz particles colliding with 304 stainless steel implemented by Tabakoffs erosion models with the coefficients mentioned in table 5.1. Transient solutions were also tested, but converged only for specimen angle at 90°.

Inlet
At the nozzle inlet, properties for water and particles is defined, given in table 6.2. The particles are uniformly distributed and have the same initial velocity as the water. Phase coupling between the water and quartz particles is one-way, which means that the particles follow the flow field without influencing on the continuous flow.

Fluid	Water and Quartz particles
Specimen angle	45° 60° and 90°
Velocity	36, 60 and 74 m/s
Nozzle diameter	8.5mm
Nozzle distance	102mm
Particle size	0.165mm
Particle density	2.6 g/cm^3
Particle mass flow	3.12 g/s

Table 6.2: Model parameters

Specimen and tank
The domain is the submerged tank filled with water. Only the specimen is defined as wall with roughness 0.31μm. The fluid exit out of the domain, thus the side of the tank is defined as openings.

Sediment concentration
When implementing particles in the simulation, only a sample of particles is calculated. Each sample represents a number of particles, and given the particle size, density and mass flow rate, the total number of particles can be calculated. For the simulations at steady state, the total amount of particles in the simulation is 510 200. In the transient simulations a total amount of particles per test run is $7.35 \cdot 10^8$, which is equivalent to an experimental test for 24 minutes and 4.5kg.

6.3 Experimental results

Castberg's experiments involve impact of quartz particles on hard metal. Results from tests with specimen is shown in figure 6.5. The specimen has been exposed 16 times by 1.5 kg sand at 74 m/s at an angle of 90°, and the measured erosion rate is $3.82g/cm^3s$. A typical erosion pattern for test at this angle is an erosion ring around the centre point. A stagnation point occurs in the centre, which will direct the fluid and particles away from the point. The erosion will then increase in the radial direction as a circle around the stagnation point. At the jet stream edge, the erosion rate decrease to zero. Due to several short runs performed on the same specimen, the centre on the specimen has vanished. For each experiment the specimen has been replaced, and only a minor variation in horizontal position can influence the result[7].
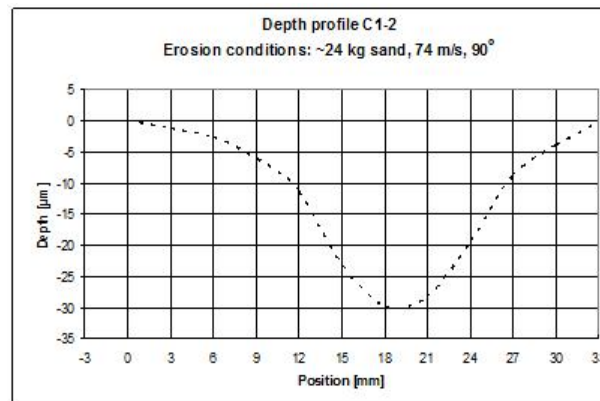
Figure 6.5: Experimental results from Castberg, erosion depth on hard metal, 90°and 74m/s

According to erosion theory, the relation between impact velocity and total erosion rate can be empirical expressed as:

$$W = KU^n \tag{6.1}$$

where
W	Erosion wear
K	Coefficient, representing all the constant properties
U	Velocity
n	Exponent value

The exponent n is highly dependent on the individual experiments, material properties and flow condition and needs to be adjusted for every experiments. From his experiments, Castberg has calculated the exponent value to be 3.33.

Results from experiments with a similar test rig is shown in figure 6.6[14]. For different impact angles, the erosion pattern and intensity is varying. At large angles, the eroded

area has a circle shape which will change to a elliptic shape with decreasing impact angle.
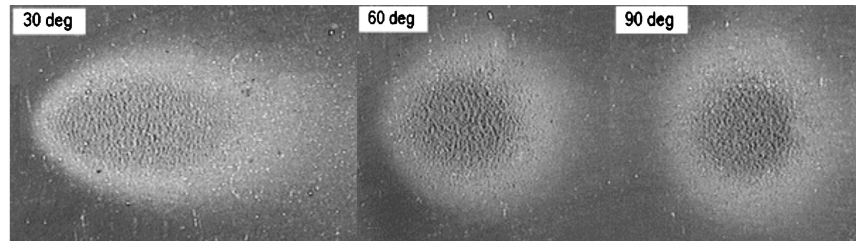

Figure 6.6: Experimental results [14]

Chapter 7

CFD model for Francis Turbine

The CFD setup of the Francis turbine simulation is treated in this chapter. Generation of grids, numerical methods and boundary conditions is defined. Basic theory is given in Appendix B.

7.1 Grid construction

Along the blade profile, an O-gird topology will give a controlled transition to the inflation layer, see figure 7.1. The mesh size is dependent on Reynolds number, turbulence model and y+ values. The y+ is a dimensionless factor which defines the distance from the wall to the first grid element.
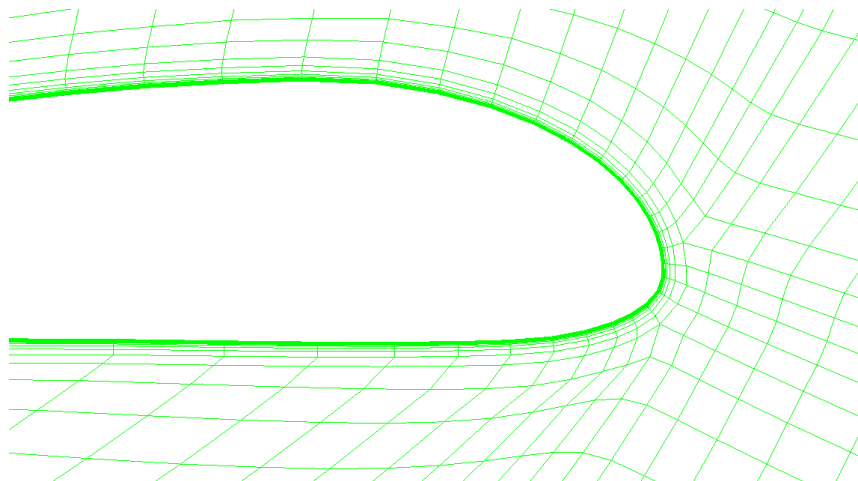
Figure 7.1: TurboGrid meshing, O-grid

The grids used in these simulations have different mesh quality, see table B. The runner

vane and guide vane is the most interesting area in the turbine, thus the mesh is larger than the stay vane. At areas were the flow includes large gradients, the grid quality needs special attention. To get a smooth transition between the small and large control volumes, an expansion factor of approximation 1.25 is recommended[1, 4].

Vane	Nodes
Stay vane	59 000
Guide vane	110 000
Runner vane	132 000

Table 7.1: Number of nodes in the grids

7.2 Numerical Model

For setting up a new simulation in Ansys CFX, a new Turbomachinery model is started. The mesh files is imported and merged together to one computational domain, see figure 7.2.

7.2.1 Boundary conditions

To simplify the simulation, only one set of blades is calculated. In the post-process, the turbine is assembled with 20 stay vanes and guide vanes, and 17 runner vanes. The two most interesting operating points are at the best point efficiency and full load, with guide vane angle of 16° and 22° respectively. To study the effect of different sediment concentration, the simulations for both operation conditions implements four different concentration rates.

Inlet and outlet
The best-practices guide from Ansys suggest to specify a total inlet pressure and mass flow outlet[3]. This will give a more appropriate calculation of the flow field than with mass flow inlet condition. The latter condition assumes an uniform inlet velocity which is not the case in a turbine. The mass flow condition is preferable since this gives more correct turbine performance values, when looking at pressure distribution, y+ values, power output, head and flow rate. Thus the inlet condition is set as mass flow rate per passage with velocity components and a constant total pressure at the outlet of the runner, see table 7.2.
Sand particles are uniformly injected at the stay vane inlet with the same conditions as the fluid. The particles will follow through the domains and exit at the outlet. The sand particles are defined as solid particles and the size distribution is uniform in diameter. The turbulence dissipation force is activated, and the Schiller Naumann model calculates the drag force acting on the particle. The coupling between the water and particles is divided into two sets, one-way coupled and fully coupled.
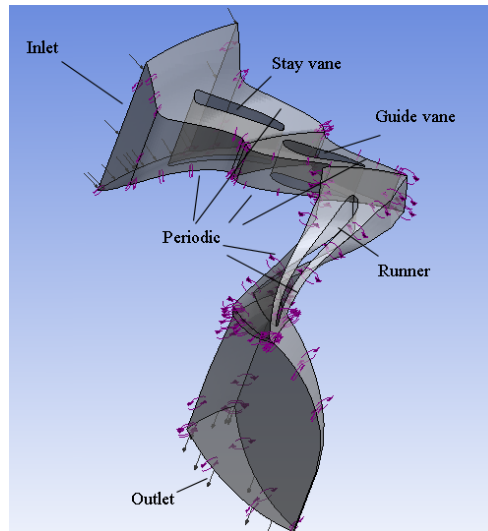
Figure 7.2: Computational model

Wall

The covers, hub, shroud and vanes are defined as smooth walls with no-slip condition. Fluid velocities near the wall will then be decreased by the wall friction. The runner has an angular velocity, ω, of 600 rpm, while the stay vane and guide vane are stationary domains. A periodic boundary condition is set to couple two adjacent blades. This simplifies the computational model and only one set of blades needs to be analyzed. To predict the erosion on the blades, a erosion model has to be selected. Two erosion models are tested in these simulations; the Finnie's and Tabakoffs erosion models

Variable	Value
Water density	997 kg/m^3
Quartz density	2,65 g/cm^3
Quartz dimension	0.1 - 0.2mm
Mass flow rate, water	540 kg/s
Mass flow rate, quartz	0.5, 3, 20, 50 kg/s
Flow Direction, stay vane inlet (a,r,θ)	0, 0.4, 0.9165

Table 7.2: Boundary conditions

7.2.2 Sediment concentration

The particle size and density is given, and when defining the mass flow rate of particles, the number of particles implemented in the simulation can be calculated. Comparing the simulated concentration with the sediment data from Cahua[8], the different concentration

Concentration rate	Tons of sediments	Equivalent to Cahua power plant
$0.5kg/s$	700	an average day during the monsoon period
$3kg/s$,	4300	a dry month
$20kg/s$	28 800	six month during the dry season
$50kg/s$	72 000	three intense monsoon month

Table 7.3: Concentration rate

rates simulated can be linked to typical amount of sediments passing the turbines at Cahua power plant.

Chapter 8

Results

8.1 Verification simulations

The CFD model is applied to analyze the jet stream from the nozzle to the specimen. After colliding with the specimen, some particles will hit the specimen again, but most of the particles vanish into the tank. Figure 8.1 shows the water jet for three angles at $74m/s$.

<div align="center">(a) 45°   (b) 60°   (c) 90°</div>
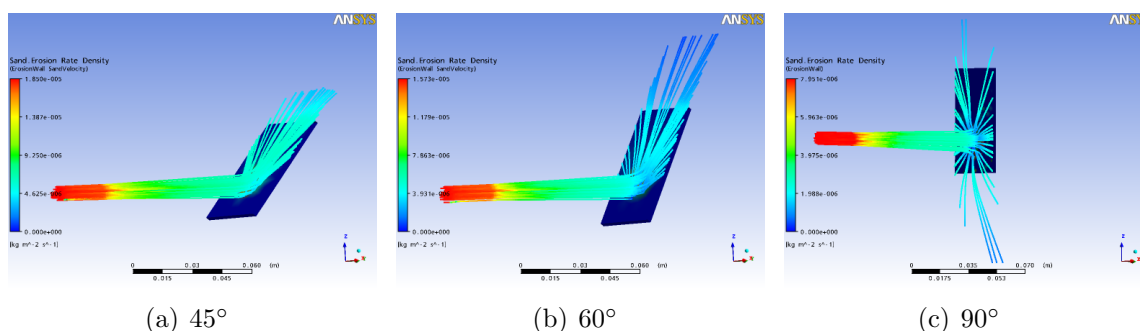
Figure 8.1: High velocity stream

8.1.1 Erosion rate versus impact angle

The impact angle is defined as the angle between the surface and the particle direction, see figure 3.1. For the simulations with an impact angle of 45° and 60° the results with jet velocity of $74m/s$ is shown in figure 8.2. The erosion pattern is similar for both angles, the particles slopes along the specimen over a large area and creates a scattered erosion pattern. The smaller the impact angle, the larger erosion area on the specimen is observed.

(a) 45°

(b) 60°

Figure 8.2: Erosion rate density on specimen at 45° and 60°

Simulations with an impact angle of 90° with jet velocity $74m/s$ is presented in figure 8.3 a. The erosion zone is shown as a concentric circles, similar to a donut. It is concentrated within an area of 20 mm, no erosion effect is observed outside this area. Figure b shows the erosion density distribution across the plate, and the donut erosion pattern is observed. The total erosion rate at this angle is $0.94g/cm^3s$.

In figure 8.4 the erosion rate for each impact angle for the different velocities is plotted. At $36m/s$, the erosion increases linearly, but for higher velocities the erosion rate is maximum at 90°.
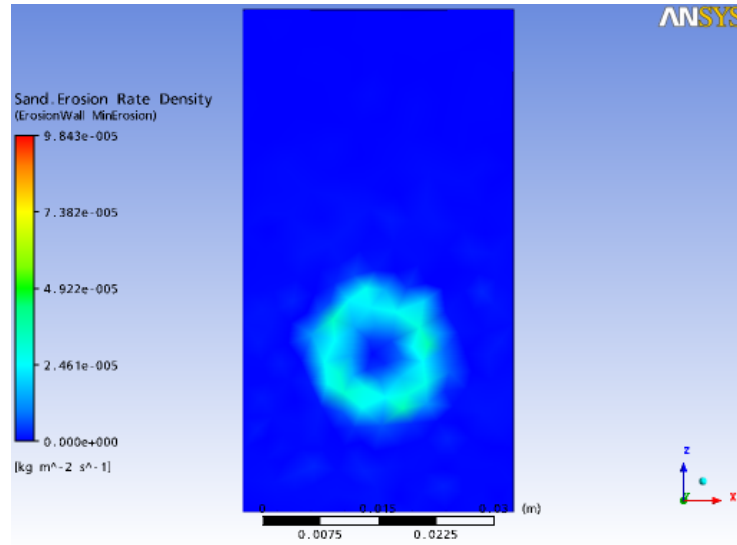
(a) Erosion rate density on specimen
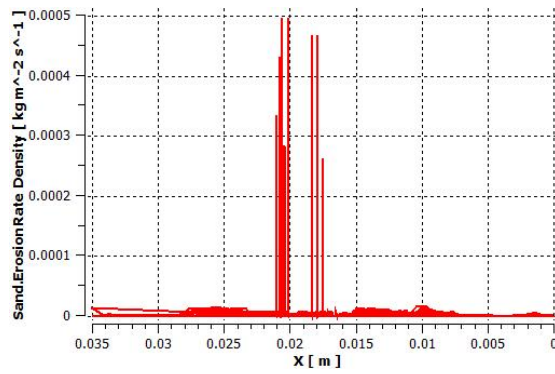
(b) Erosion distribution across the specimen

Figure 8.3: Erosion rate on specimen 90° and at $74m/s$
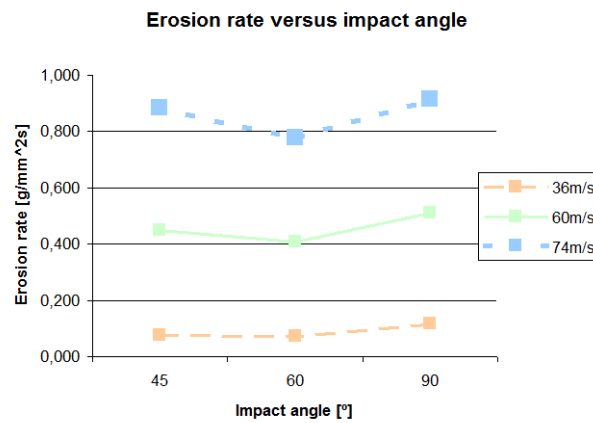
Figure 8.4: Erosion rate versus impact angle

8.1.2   Erosion rate versus velocity

The effect of velocity on erosion rate is presented in figure 8.5 for a specimen at 60°. All analysis have fixed parameters, except from the velocity. The vertical colour bars to the left in the figures have the same scale, and the development of erosion due to increasing impact velocities is seen.

In figure 8.6, the erosion rate for each angle is plotted for three velocities. The erosion rate increases linearly for all impact angles. From this graph, the exponent n can be calculated and is presented in table 8.1.

Impact angle	n
45°	2,27
60°	2,22
90°	1,90

Table 8.1: Exponent values from simulations with Tabakoffs erosion model

In figure 8.7 a, a counter plot of the slurry velocity is given. The maximum velocity of the water is at the nozzle outlet, and gradually decrease closer to the specimen. Figure 8.7 b shows the sand velocity $0.01mm$ from the specimen. The jet diameter has expanded to 22mm, and within this diameter the particles collides on the specimen with a velocity between $3m/s$ and $18m/s$. The blue dot in the middle of the jet, is a dead zone where particles has a velocity around 2-$3m/s$.
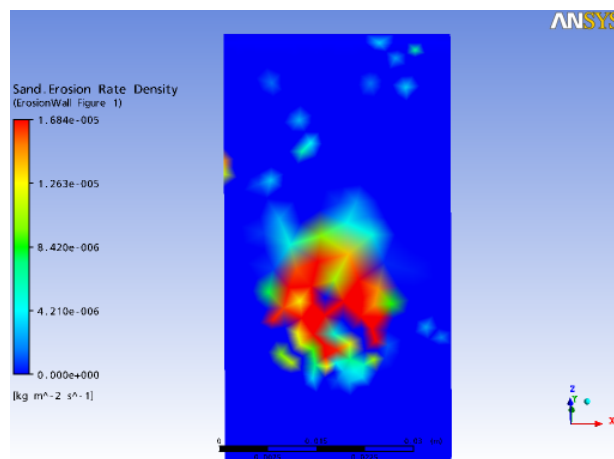
Right after collision, particles bounce out and the velocity reach up to $30m/s$, and then decreases along the specimen surface, see figure 8.8. Outside this area, velocity still decreases and particles vanish out of the domain. Some particles collides a second time, but with a low impact angle and insignificant erosion is observed.
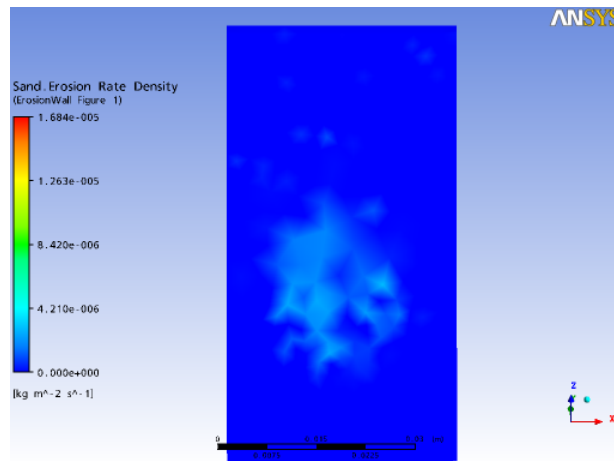
(a) 30m/s
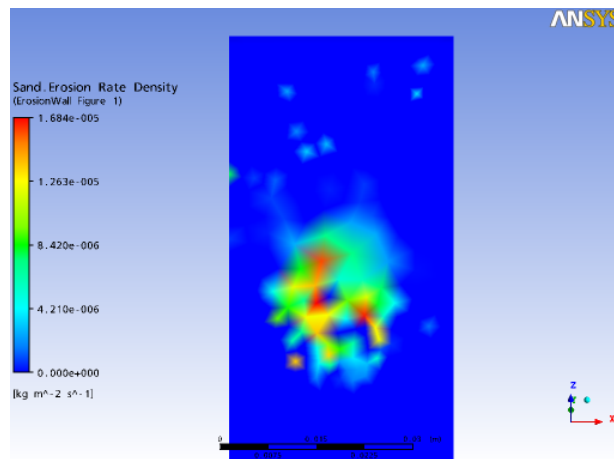
(b) 60m/s

(c) 74m/s

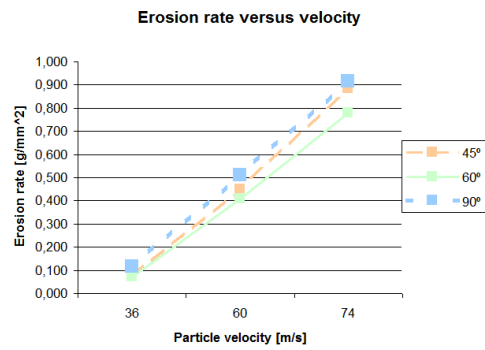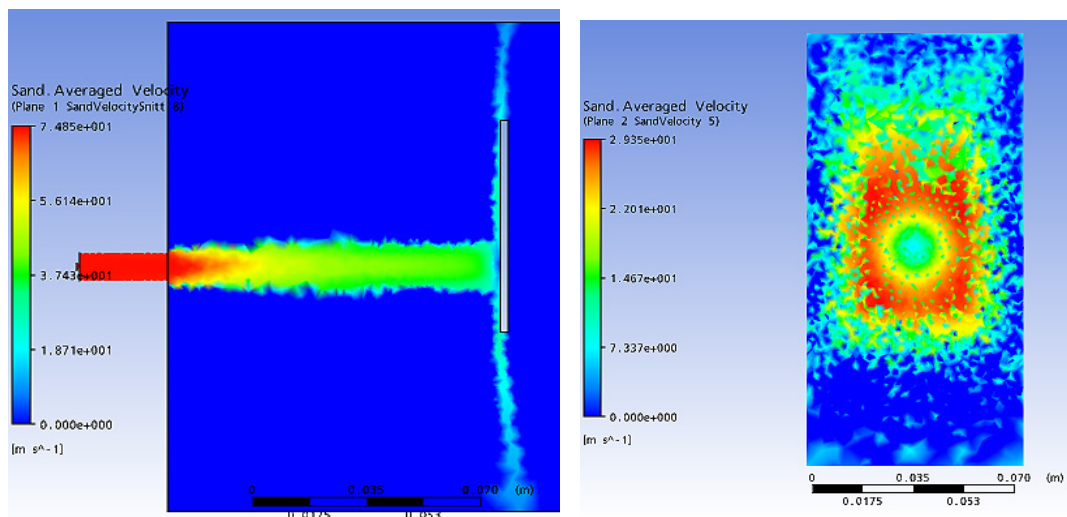Figure 8.5: Erosion effect for different velocities

Figure 8.6: Erosion rate versus velocity

(a) Sand velocity distribution from nozzle to specimen

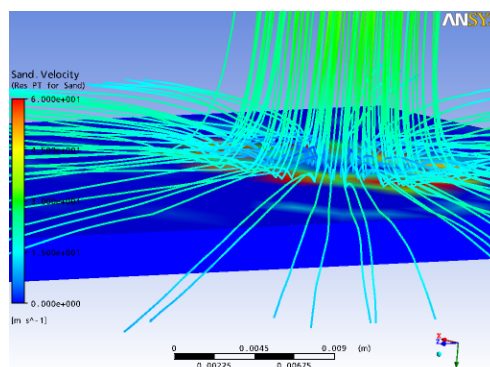(b) Sand velocity 0.01mm from specimen

Figure 8.7: Sand velocity

Figure 8.8: Colliding particles at specimen

8.2 Sediment erosion in Francis turbine

In this section, the results from the simulations is presented. Firstly, looking at the potential erosion areas and then a concentration study follows. Two erosion models are tested for two operation points, best efficiency point(BEP) or design load, were the guide vane angle is 16°, and full load with guide vane angle 22°. Since the erosion pattern for the different erosion models looks similar, only results from Tabakoffs erosion model are presented.

8.2.1 Erosion areas

The erosion models calculates the forces that acts when the particles collides with the wall. The erosion rate indicates loss of material per square meter per second, and are seen as coloured spots. This indicates the erosion intensity, were blue denote zero erosion and red is high erosion intensity. Detection of erosion areas at the three blades are presented, comparing design load and full load for different mass flow rates.

Stay vane

Figure 8.9 a, indicates erosion zones at the stay vane. Especial close to the upper and lower area of the leading edge, the erosion intensity is higher than in the middle. Erosion spots on the blade suction surface are observed, but the pressure side has no indication of erosion. At the spiral casing transition to the vane, spotted erosion occurs with varying intensity. Figure 8.9 b demonstrates the sediment flow velocity around the stay vane.
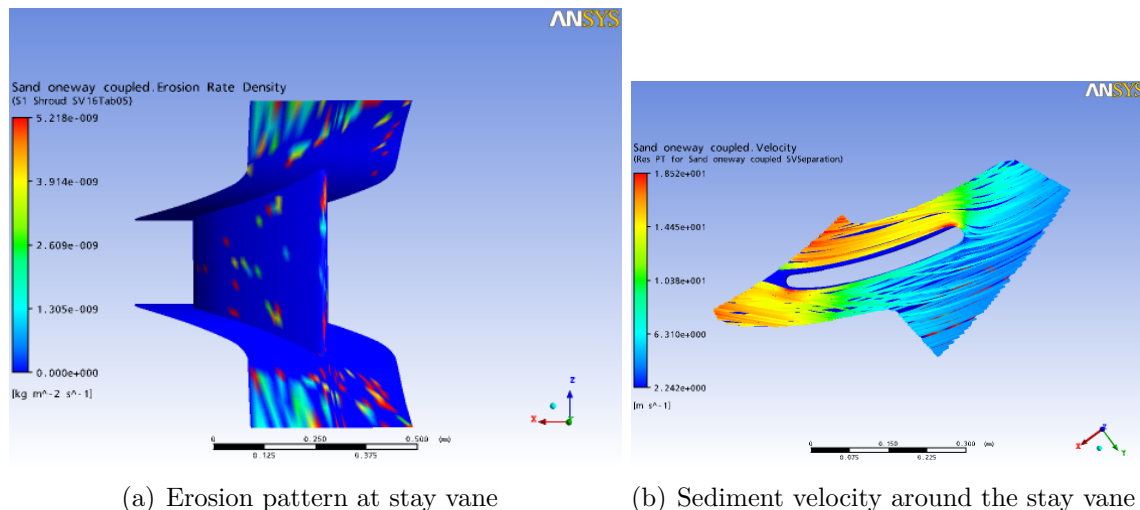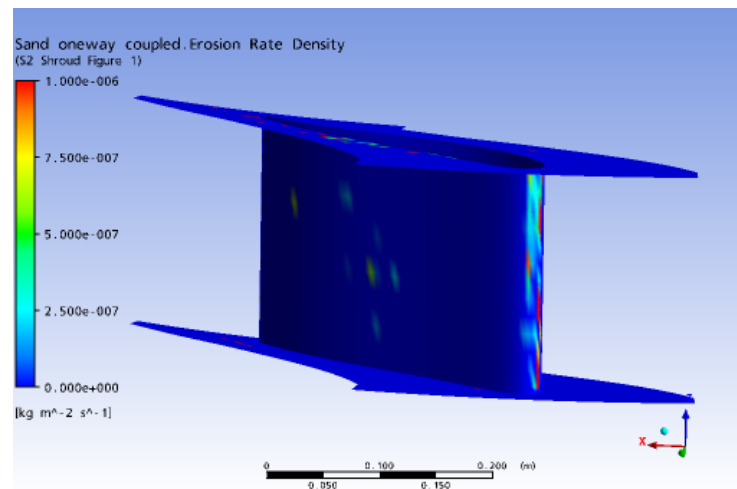

(a) Erosion pattern at stay vane   (b) Sediment velocity around the stay vane

Figure 8.9: Flow condition at stay vane, BEP

Guide vane

The erosion tendency at the guide vane is displayed in figure 8.10. At design point, the leading edge is the most exposed erosion area. Some erosion spots on the blade pressure side is observed, but the suction side has no erosion. Along the pressure side of the blade, erosion is detected at the facing plates. Only minor erosion effects is observed at the lower cover compared with the hub. Operation at full load indicates similar erosion tendency. The erosion spots are smaller, but with higher erosion intensity than at design point. At the suction side, few erosion spots are observed on the facing plates. The particle velocity around the guide vane is seen in figure 8.11.

(a) Erosion on guide vane at design load
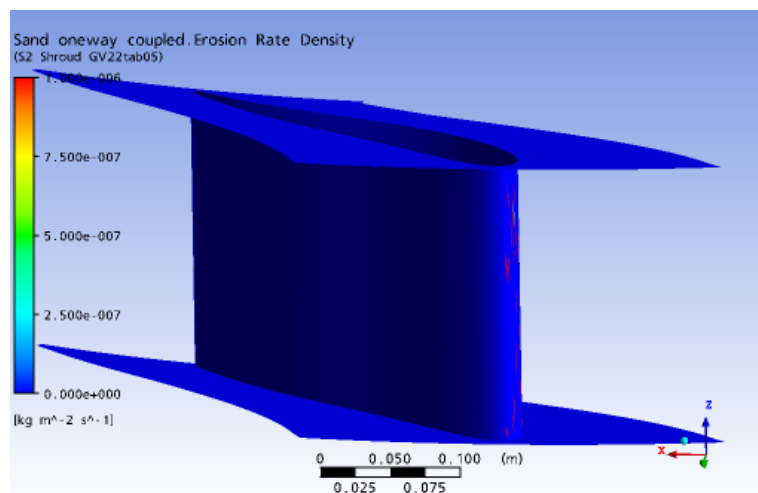
(b) Erosion on guide vane at full load

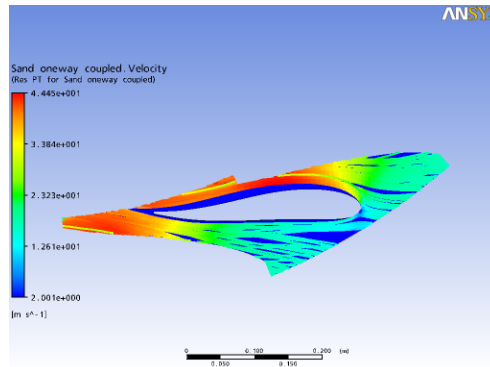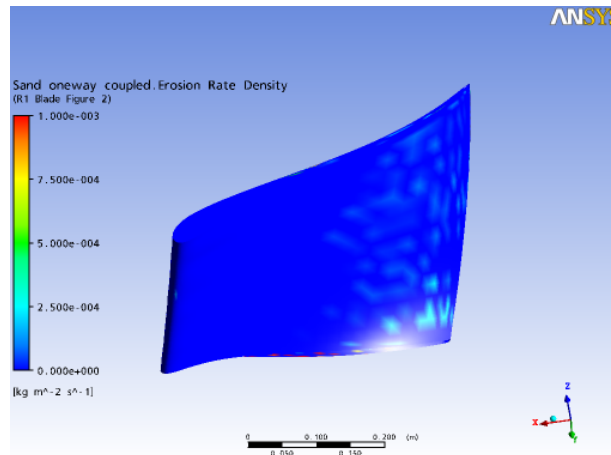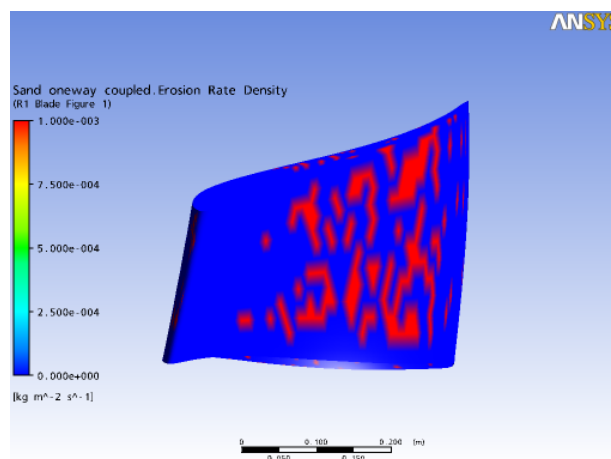Figure 8.10: Erosion tendency at guide vane

Figure 8.11: Sediment flow velocity at guide vane

Figure 8.14 shows the erosion pattern at the hub and shroud for both operation points. Near the blade root at runner inlet, erosion grooves seems to occur at design load. The intensity of erosion is increasing in the channel closer to the outlet area, especially at the hub. For full load operation, erosion intensity is higher in the channel than at the inlet area.

Looking at the particle flow around the blade at design load, see figure 8.15, the particles seems to first hit the pressure side and then cross the channel and hit the next blade, especially near the shroud. At the full load operation, the major part of the particle tends to seek to the middle and then towards the shroud. Figure 8.16 illustrates the pressure distribution at design load.
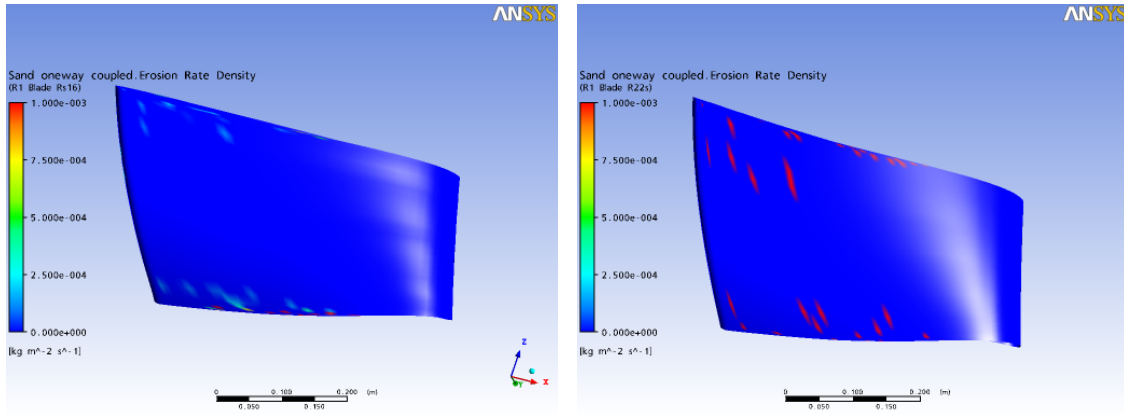
(a) Erosion on runner vane at design load

(b) Erosion on runner vane at full load

Figure 8.12: Erosion tendency at runner vane, pressure side

Runner blade

As seen in figure 8.12 and 8.13, minor erosion spots are detected at the leading edge. The runner is most exposed for erosion at the outlet area on the pressure side. At BEP the erosion spots is detected at the middle of the blade and towards the outlet area. Same erosion areas is seen at full load operation, but with an higher erosion intensity. Both for design load and full load simulations, erosion occurs at the upper and lower part of the outlet area on the suction side of the blade.

(a) Erosion on runner vane at design load   (b) Erosion on runner vane at full load
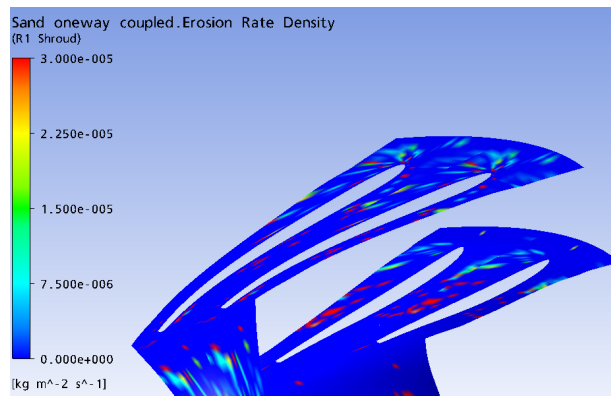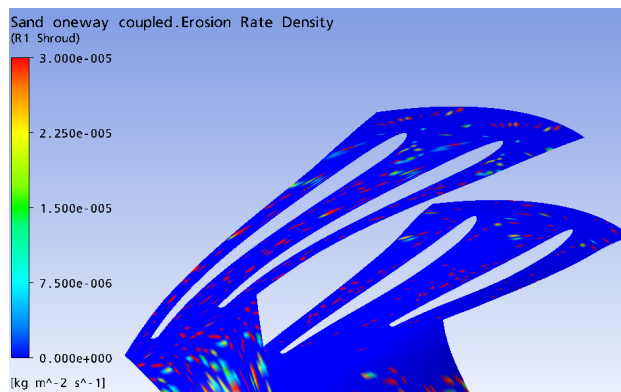
Figure 8.13: Erosion tendency at runner vane, suction side

(a) Design load

(b) Full load

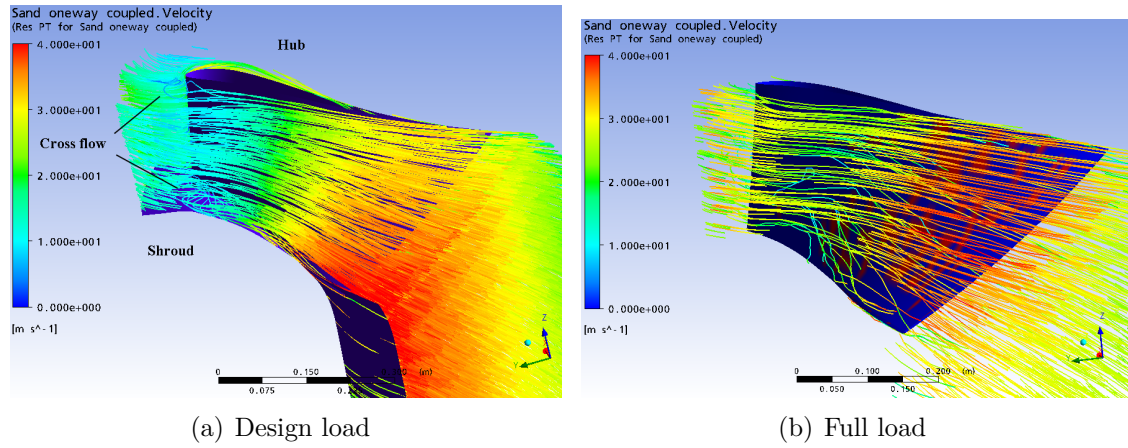Figure 8.14: Erosion on hub and shroud at runner

(a) Design load

(b) Full load

Figure 8.15: Particle flow around the runner vane
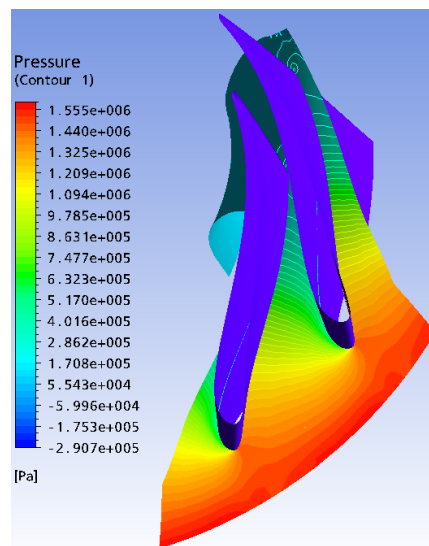
Figure 8.16: Pressure distribution on the runner vane at design load

8.2.2 Concentration study

Comparison between Finnies and Tabakoffs erosion models are presented in the following figure 8.17. The graphs indicates the erosion tendency for different sediment concentration for full load and design load for one runner blade. Take notice to the z-axis on the graphs which indicates the erosion rate.
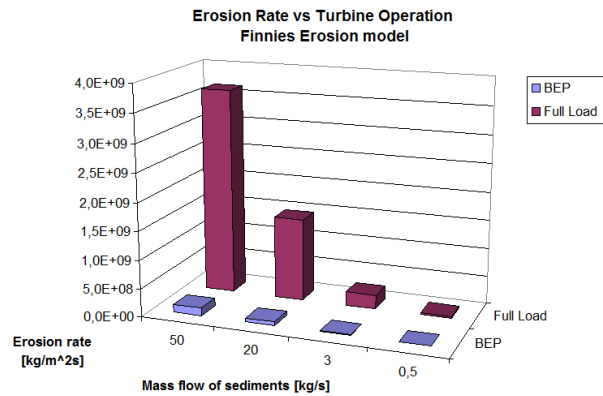
(a) Finnie's erosion model
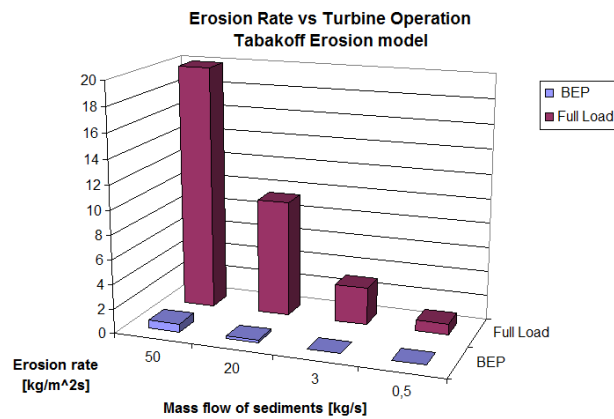
(b) Tabakoffs erosion model

Figure 8.17: Finnie's and Taboffs erosion rate for Francis turbine

Figure 8.18 shows the concentration rate at BEP for a low and high sediment concentration. Near the shroud at the runner outlet, the erosion pattern starts to develop for low concentration and intensify with increasing concentration.
Erosion development at full load operation is demonstrated in figure 8.19. Larger erosion spots are detected at the blade surface compared with design load, and the intensity is higher.
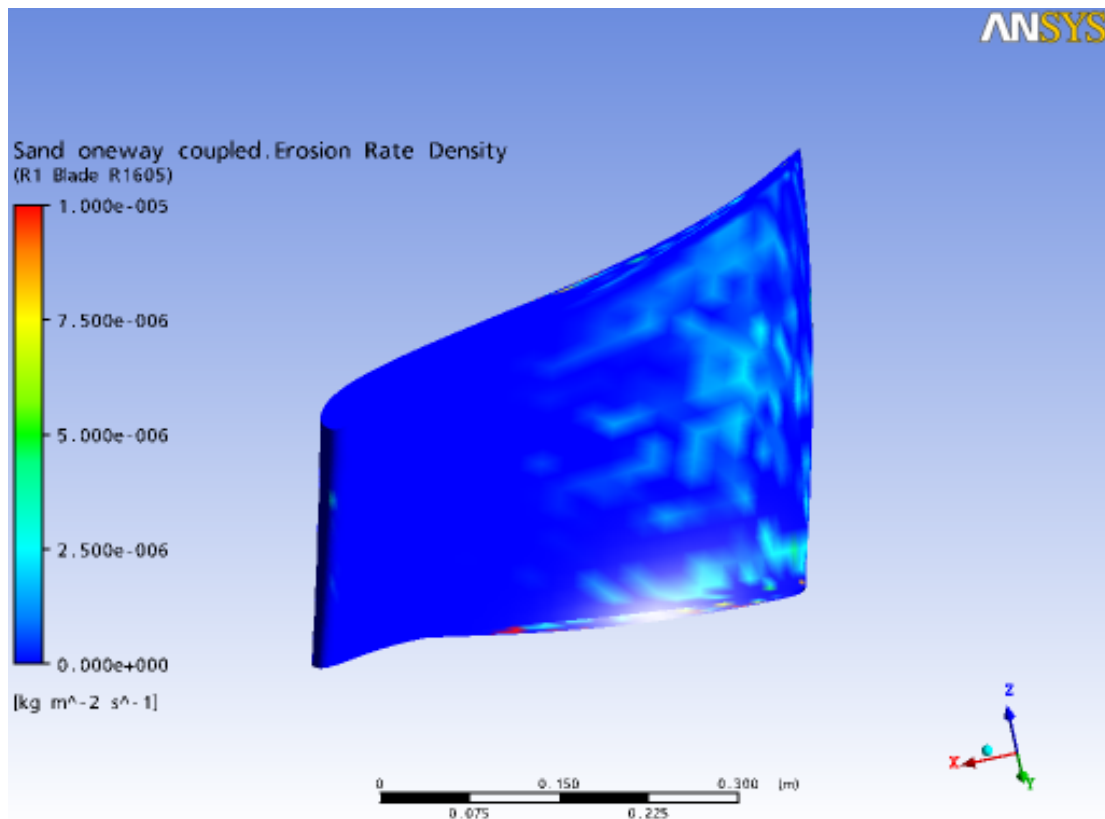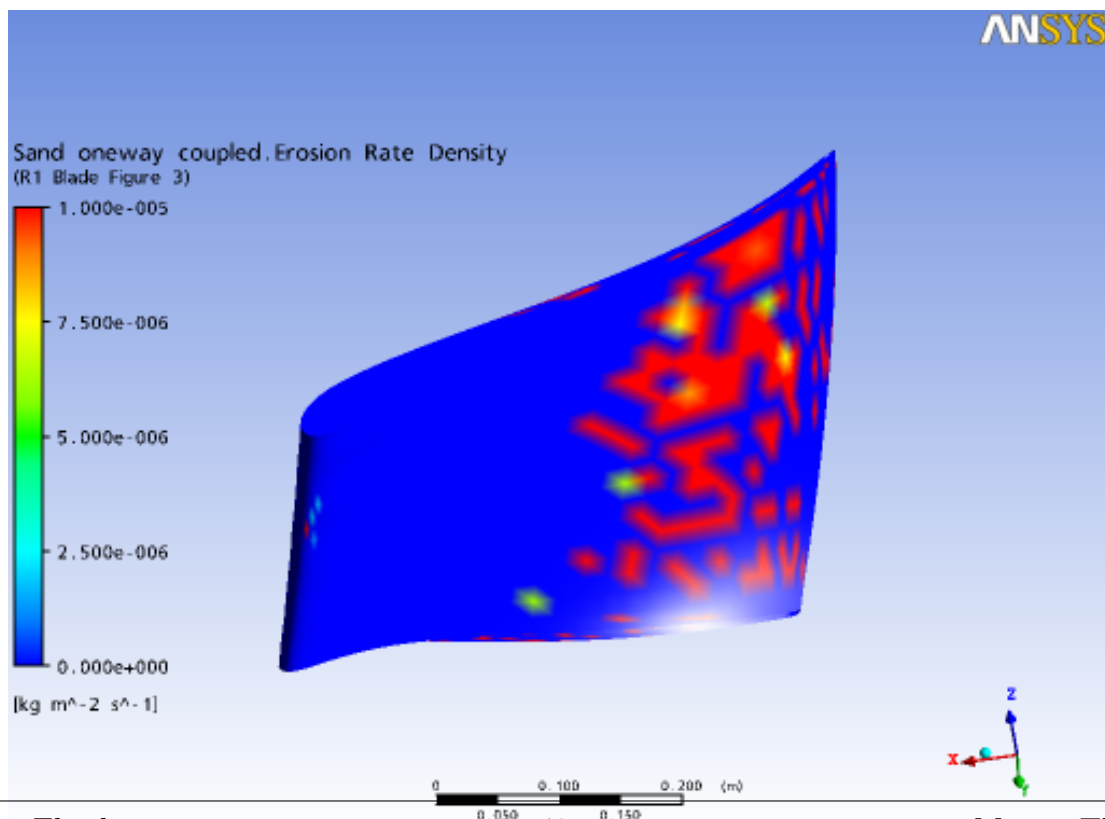
(a) $0.5 kg/s$

(b) $20 kg/s$

Figure 8.18: Erosion at runner for low and high sediment concentration rate at design load
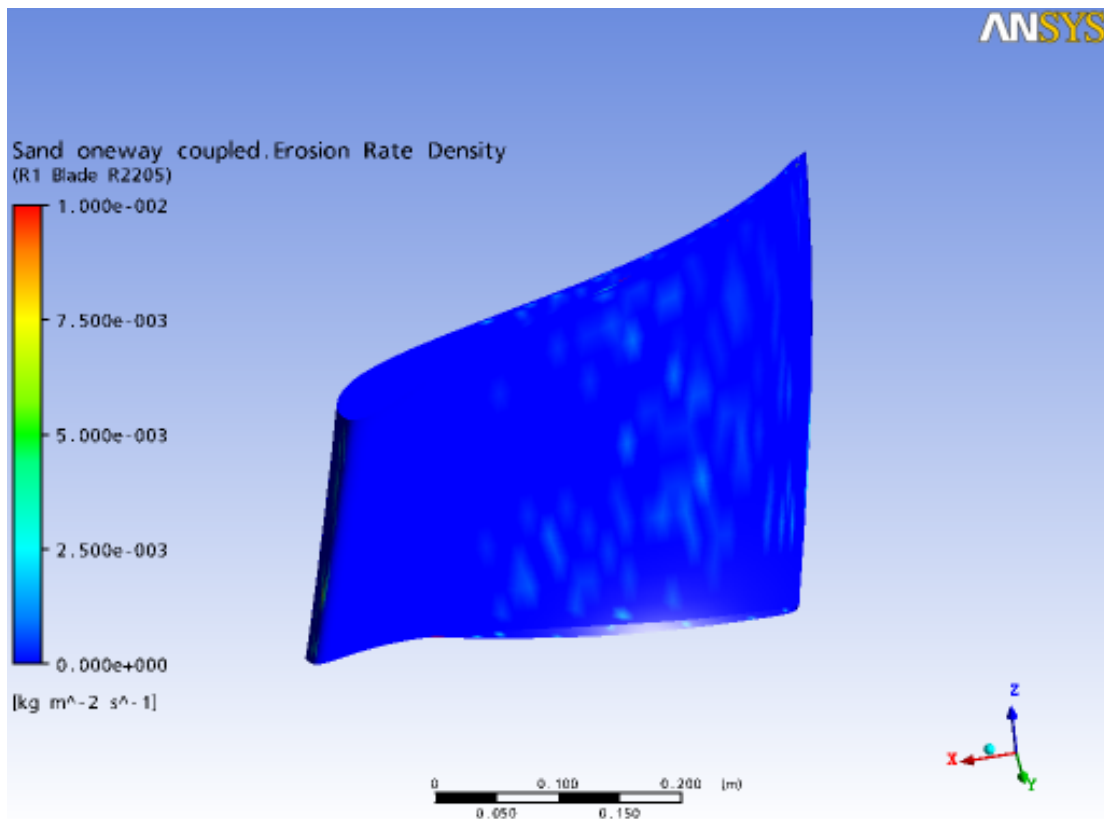
(a) $0.5 kg/s$
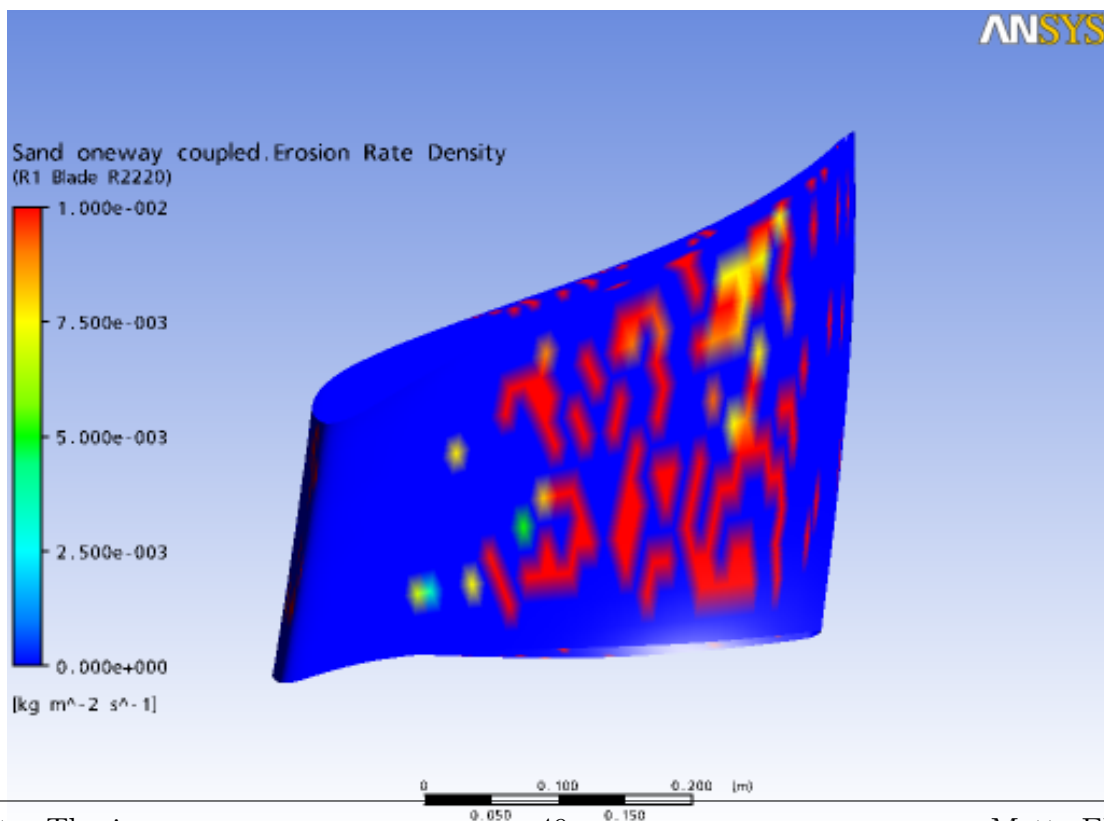
(b) $20 kg/s$

Figure 8.19: Erosion at runner pressure side at full load operation

Chapter 9

Discussion

The intension of the comparison between the verification model and experiments from Castberg, was to prove that the erosion models and simulations can predict erosion areas and intensity.

9.0.3 Erosion rate versus impact angle

The simulations indicate erosion for specimen at three angles, 45°, 60° and 90°. For low angles, the erosion pattern will disperse over a larger area, and the erosion pattern occurs, as seen in figure 8.2. Transient simulations will implement an amount of particles closer to what is utilized in the experiments. Results from these simulations at these angles would have given a smoother erosion pattern and look closer to and ellipse.

At 90°, the erosion pattern on the specimen appear as a "halo ring". Comparing the simulations with results from Castberg, see figure 6.5, the *erosion pattern* is similar for specimen at 90°. In Castbergs experiments, the centre of the erosion point has vanished, due to replacement of specimen after several test runs. Also in figure 6.6 the same erosion tendency is observed.

In comparison with experiments, the *erosion rate* for 90° gives no similarity. This is probably due to the material properties. The simulations involve the erosion effect on a ductile material, 304 stainless steel, but the experiments involves with a hard and brittle metal. Thus the rate of erosion can not be compared, but regarded as a relative expression for the erosion intensity. The effect of erosion on brittle and ductile materials in shown figure 3.2. The same relation is plotted in figure 8.4 for three velocities. The curves should look similar to ductile materials, were the erosion rate is maximum for low angels (10°-30°) and decreasing with higher impact angles. High erosion occurs at 90°, which is not correct according to the theory about ductile materials.

9.0.4 Erosion rate versus velocity

The erosion rate for different velocities is seen in figure 8.5. As expected, the erosion rate increases with higher velocities. The development of the erosion pattern is easily seen, and the red areas are the most exposed zones. The erosion rate is also shown for all angles in figure 8.6. From these curves, the values for the velocity exponent, n, are calculated for each angles, given in table 8.1. According to ductile material theory, the values agrees, as the value decrease with increasing angles[7]. Simulations implementing Finnies erosion model were also tested. Only the value for the exponent needs to be defined in this model. When inserting Castergs exponent value, 3.33, the calculated erosion rate was unrealistically large since the model only depends on this exponent value and gives a over estimated erosion intensity. Thus the Tabakoffs erosion model was utilized for these simulations.

The velocity profile from the nozzle outlet to the specimen is showed in figure 8.7 a. The jet stream has a velocity of $74m/s$ out of the nozzle, but reduces to $15m/s$ at the specimen. This is due to friction in the water. The effect of this decrease in velocity can be observed in the erosion pattern in figure 8.3. The particles have a normal impact angle, but due to the low velocities in the stagnation point, minor erosion occurs at this point.

9.1 Sediment erosion on Francis turbine

9.1.1 Erosion areas on the blades

Stay vane
The prediction of erosion at the stay vanes has similarities with the theory. As mentioned in chapter 4.3, the erosion occurs at the leading edge close to the hub and shroud, see figure 8.9. The area in the mid height of leading edge has minor erosion intensity. On the blade surface, scattered erosion spots are observed at pressure side. On the suction side, no erosion occurs, this is due to the boundary layer effect which is see figure 8.9 b. As mentioned in the CFD theory, chapter 5, this effect is one of the limitations in many turbulent models. Especially the k-ϵ has limitation when it yields flows over curved surfaces and boundary layer separation. Simulations with the SST turbulence model also shows the same tendency, although the model utilizes a better and more robust function to calculate the flow near wall. The boundary layer effect may be due to the initial velocity values at the stay vane inlet or incorrect mesh properties. The stay vanes at Cahua have been through several monsoon periods, and the most vulnerable areas is often welded and repainted, seen in the picture from Cahua, figure 4.1. Results from the simulations indicate similar trends at the leading edge and blade surface.

Guide vane
The simulations indicates minor erosion on the guide vane, see figure 8.10. The blade surface has spotted erosion on the pressure side, but since the absolute velocities and acceleration increases, the erosion intensity should be higher. Also at the guide vane, the boundary layer effect occurs and the particles do not collide on the suction side, and therefore no erosion occurs. Minor erosion spots appear at the lower cover. At the upper cover more erosion spots occurs at the blade pressure side. The leading edge is not an exposed area according to theory and the observation at Cahua power plant, however, the simulations indicates erosion at the entire leading edge. This poor erosion prediction can be due to poor grid density or incorrect input values, which affects the flow conditions.

Runner vane
Since the simulations are steady state, the erosion effect in the runner is highly dependent on the fixed runner placement. Transient simulations will give a more realistic prediction of erosion, but due to limitations in the software this were not feasible. At the inlet area, minor erosion is observed for best efficiency point, but at full load the erosion intensify and more spots are found. This can be due to differences of flow angles coming from the guide vane. Due to increasing relative velocities in the runner channel, the erosion intensity will increase from the middle of the blade towards the outlet area. This effect is larger at full load operations. At the runner inlet, the pressure distribution will interrupt the particle flow and the flow tends towards the low pressure side. The particles crosses the channel and make grooves at the hub and shroud. Especially at full load, where the centrifugal forces are larger, the particles are extracted against the upper and lower cover and the

erosion intensify. This effect is observed from earlier experiences 4 and at inspection at Cahua power plant.

9.1.2   Erosion concentration studies

The results clearly shows that the concentration of sediments will influence the erosion intensity on the turbine, see figure 8.17. At design load, the erosion gradually increases along with the sediment concentration. Other tendencies appear at full load, where the erosion rate is growing drastically with higher sediment concentration. For small concentrations, the rate is almost similar for both operating points.

The figure 8.17 shows the erosion rate predicted with the two erosion models. The Finnies erosion model gives erosion values around E+08, which is improbable, since a turbine exposed to such an erosion would fall into pieces. Simulations with Tabakoffs erosion model give a more realistic erosion rate. Disregarding the absolute erosion rate, the erosion development is similar for the models. At full load, the erosion rate grows fast with increased concentration. This may not be the case for best point operation. The same appears for the Finnies erosion model. This signifies that the erosion rate at design load is not that crucial for the turbine.

The quantity of particles passing the turbines at Cahua power plant is known, and these values is possible to implement in the simulations. Results from these simulations indicate erosion after one day, one month, half a year and a monsoon period with high sediment concentration. Thus it is possible to predict when the turbine needs maintenance. The only mineral implemented in the simulations is quartz. For the real case in Cahua, the river contains about 30% of quartz. To get a better erosion rate prediction, the exact amount of the different minerals should be included.

The results indicates growing erosion rate with increased operation load, but this will not be the case for all power plants. Even if the concentration rate and mineral contents are the same for two similar turbines, the erosion areas and intensity can be quite different[6]. This illustrates how complex the sediment erosion in turbines can be, and it is difficult to handle the problem concerning each individual power plant, its best load and maintenance schedule.

9.2   Theoretical models versus numerical erosion models

Both Finnies and Tabakoff erosion models are tested in the simulations, but indicate dissimilar values for erosion rate. This can be explained with the mathematics behind the models. The most influencing factors in the models are the velocity and material constants.

In Finnies erosion model, the exponent,n, is highly dependent on the individual experiments and material properties. For Francis turbines, the exponential value is recommended to be 3[15], but in Ansys Solver Guide[3], a value between 2.3 and 2.5 for steel material is suggested. The simulations implementing Finnies erosion model are tested for all these values, but the erosion prediction is unrealistic. The experiments done by Castberg is on brittle material, and the exponent value from these tests is calculated to be 3.33. When inserting this value into the simulations, the erosion rate is extreme large and not comparable with the experiments.

In Tabakoffs models, the values for 304 stainless steel are implemented, which is a ductile material. Since the material in Castbergs experiments is a brittle metal, the erosion rate is not comparable with the simulations. Anyhow, the simulations with this model calculate a more realistic erosion rate value than with Finnies model. When it comes to the simulations with the Francis turbine, the results with Tabakoffs erosion models will give a more realistic erosion rate indication than the Finnies erosion model. The simulation takes into account the influence of quartz particles colliding with the ductile material. This prediction is closest to the uncoated turbine at Cahua power plant because of the properties of the material.

For every numerical model, the theoretical erosion models needs to be modified and adjusted to the exact problem. Theory and experiments can indicate important values for the input variables, but verification models are needed to confirm the simulations.

Chapter 10

Conclusion

The analysis of sediment erosion in Francis turbines gives an indication of relative erosion intensity and zones. The results coincide with earlier experiment and observation at the turbine in Cahua. The simulations for the runner gives the most realistic prediction of erosion. Especially at hub and shroud near the blade roots, and the outlet area on the blade, the most serious erosion occurs in the turbine.

A study on the concentration effect of sediment indicates the erosion development in the turbine. At low concentrations, the most exposed areas will first be visible, such as the outlet area of the runner. This indicates the critical erosion zones which first will need reparation. Simulations with a higher concentration rate will indicate the growing erosion intensity near the vulnerable areas. By changing the concentration rate in the simulations, it is possible to predict when the turbine components require maintenance.

An correlation between CFD and data from experiments and experiences is presented. Results from the simulations on the verification model shows similarity with experiments when comparing the erosion tendency. Due to the erosion models and material properties, the degree of erosion intensity is incorrect. After testing two erosion models, the Tabakoff erosion model is the most suited erosion model for these simulations. The model indicates erosion tendency closer to the reality, compared to Finnies erosion model. A modification of the numerical erosion model, adjusted for the particular problem and for which material that is utilized, will give a better prediction of erosion intensity.

Chapter 11

Further Work

PhD student Hari Neopane is working on a doctoral theses about Quantification of Sand Erosion in hydraulic Machinery. CFD- analysis about sediment erosion in Francis turbines are also a part of the theses, where he will do a deeper study on how the particle size, shape and concentration influence the erosion intensity in the turbine.

To get a better prediction on erosion rate, the erosion models can be modified with a Fortran code implementing the properties for Wolfram Carbide.

By including the spiral casing, a better simulation of the flow distribution will be achieved.

It is of interest to look at the effect of leakage flow and sediment erosion. When generating the grids in TurboGrid, a clearance can easily be added on the guide vane.

A transient solution gives better erosion prediction, but is not supported in Ansys CFX version 11.0.

Bibliography

[1] CFD online. `www.cfd-online.com`, 260509.

[2] Material Property Data. `http://www.matweb.com`, 310605.

[3] Ansys CFX Release 11.0. *ANSYS CFX-Solver Theory Guide*. December 2006.

[4] Ansys TurboGrid Release 11.0. Users guide. December 2006.

[5] Tri Ratna Bajracharya. *Efficiency Deterioration in Small Pelton Turbines due to Sand Particles Led Bucket Erosion*. PhD thesis, Tribhuvan Universtiy, Nepal, 2007.

[6] A. R. G. Rao C. V. J. Varma, B. S. K. Naidu. *Silting Problems in Hydro Power Plants*. 1st International Conference, Central Board of Irrigation and Power, India, 1999.

[7] Tore Castberg. Personal conversations, 2009. PhD student, College in South Trøndelag, HiST.

[8] Henry P. Cáceres. Personal conversations, 2009. Plant Manager, Cahua power plant, SN Power, Peru.

[9] H.Stølen E.Tesaker D. Lysne, B. Glover. *Hydraulic Design*. Hydropower Development, Norwegian University of Science and Technology (NTNU), 2003.

[10] C. G. Duan and V.Y. Karelin. *Abrasive Erosion and Corrosion of Hydraulic Machinery*. Series on Hydraulic Machinery - Vol. 2, Imperial College Press, 2002.

[11] Mette Eltvik. *Sediment Erosion in Francis Turbines*. Master's thesis, Norwegian University of Science and Technology (NTNU), 2008.

[12] SN Power. Presentation of the energy situation in South America, 2009. SN Power office, Santiago, Chile.

[13] SN Power. Fact sheet: Cahua Hydropower Plant. `http://www.snpower.no/Our_business/Latin_America/SN_Power_in_Peru/peru/Cahua_factsheet.korr.pdf`, 310509.

[14] W. Tabakoff R. Wenglarz, A. Hamed. Erosion and deposition in turbomachinery. *Journal of propulsion and power*, 2006.

[15] IEC62364 rev.7. *Guide for dealing with abrasive erosion in water.* 2008.

[16] S.K Singal and Ratnendra Singh. Impact of silt on hydro turbines. *Himalayan Small Hydropower Summit*, Oktober 2006.

[17] Bhola Thapa. *Sand Erosion in Hydraulic Machinery.* PhD thesis, Norwegian University of Science and Technology, NTNU, 2004.

[18] H. K. Versteeg and W. Malalasekera. *An Introduction to Computational Fluid Dynamics, second edition.* Pearson Education Limited, 2007.

Appendix A

Sediment Erosion Theory

Theory in this chapter is taken from [17]

A.1 Erosion wear

According to Thapa[17], wear can be defined as:

> " the rate of material removal or dimensional change due to wear per unit of
> exposure parameter, for example, quantity of material removed (mass, volume,
> thickness) in unit of sliding or unit of time."

Sediment in rivers can be composed of clay, silt, sand and gravel where the size range vary
from 0.002mm to 60mm. Transportation of sediments in rivers are classified as bed load
or suspended load depending on how the particles interact with the water. Suspended
load has nearly the same velocity as the water whereas bed load velocity is slightly slower
and will slide, roll or jump along the wall. The simulations in this project apply sediment
particles with an average size of 0.1 mm which is classified as suspended load.

A.1.1 Particle Velocity

For calculating erosion rate the particle velocity is a very important factor, but it is difficult
to obtain accurate measurements. Still, particles with low velocities which have too little
kinetic energy to induce abrasive erosion can cause erosive wear like fatigue and elastic
deformations. [17]

$$Erosion \propto Velocity^n \tag{A.1}$$

The recommended erosion expression involves the particle velocity and a factor n that
takes into account the material used and operation conditions. Different studies indicate

values of n between 1 and 5 but in view of the kinetic impact energy as a result of erosion, a factor 3 is used.

A.1.2 Impact angle

The angel between the surface and the particle path shortly before impact is called the impact angle (see figure A.1). For an impact angle near 0 degrees the particles slides parallel to the wall and erosion can be detected. For increasing angles, different erosion occurs depending on material type.
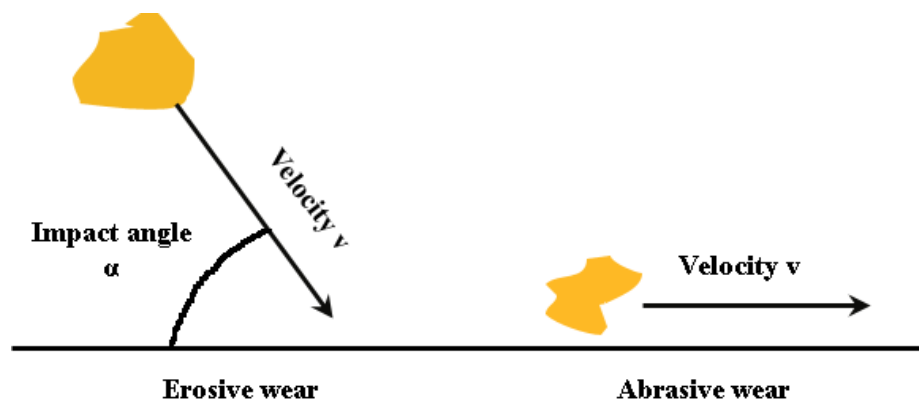

Figure A.1: Erosion Mechanisms

A.1.3 Particle Mechanisms

Sand particles follow the velocity stream and attack the surface of the material with a certain velocity and angle. Two abrasive mechanisms indicate erosion, depending on how particles attack the material.

- Erosive wear, impact erosion. Particles hits the material with a velocity v and an angle α, and over time material will be removed due to deformation, cutting, fatigue cracking or a mix of these.

- Abrasive wear, sliding erosion. A bed of particles slides over the surface with a velocity vector parallel with the surface, minor parts of material will be removed.

A.2 Sand properties

Erosion rates depends on fluid conditions such as velocity and turbulence, particle transport mechanisms and particle properties. In this section the different physical properties like hardness, shape, size, concentration and density will be discussed.

A.2.1 Hardness

Hardness of minerals is represented in Mohs hardness scale where diamond has the factor 10, talc 1 and quartz 7 [**?**]. When particles are harder than the turbine material, serious erosion takes place. Hardness and shape can be connected together when looking at erosion impact. Soft and spherical shaped particles will not create as much erosion as hard and sharp particles. Quartz particles have an angular shape and high hardness factor and will therefore cause a rough damage [16].

A.2.2 Shape and size of particles

The particle shape is essential for the erosion rate, whereas a round shape cause less damage than a particle with sharp edges.
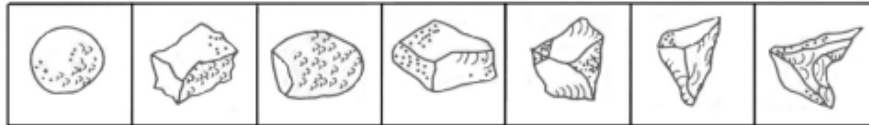

Figure A.2: Sand shape

Thapa mentions an observation done by Sheldon and Finnie on erosion due to particle size. Large particles induce erosive wear and the erosion rate is dependent on the material toughness. Small particles have a higher abrasive erosion effect and the rate of erosion depends upon the hardness of the material.

A.2.3 Concentration

The concentration is the amount of particles in a fluid given by part per million (PPM), which also can be termed [$mg/litre$]. Generally a large concentration amount gives higher erosion rate. Some authors have done tests on the effect of concentration, but results a varying[5]. As a conclusion, the concentration as function of velocity is a suitable approximation of the erosion rate.

Appendix B

CFD

The CFD analyse is of the sediment erosion was performed by using Ansys CFX 11.0. Firstly a mesh of the geometry had to be made before setting the fluid conditions for the simulation. This chapter will give some background of the theory behind CFD, generating grids and setting up an analysis. Theory in this chapter is taken from [3], and [18].

B.1   CFD Theory

B.1.1   Basic equations

Fluid dynamics is based on three fundamental principles which are Newtons 2.law, mass- and energy conservation. These principles are difficult to solve analytically and are therefore described with partial differential equations;

The Continuity Equations:

$$\frac{\partial \rho}{\partial t} + \Delta(\rho U) = 0 \tag{B.1}$$

The Momentum Equations:

$$\frac{\partial \rho U}{\partial t} + \Delta(\rho U \cdot U) = -\Delta p + \Delta \cdot \tau + S_M \tag{B.2}$$

where τ is the stress tensor and S_M is the momentum source.
The Total Energy Equation:

$$\frac{\partial \rho h_{tot}}{\partial t} - \frac{\partial \rho}{\partial t} + \Delta(\rho U h_{tot}) = \Delta(\lambda \Delta T) + \Delta(U \cdot \tau) + U \cdot S_M + S_E \tag{B.3}$$

where h_{tot} is the total enthalpy, $\Delta(U \cdot \tau)$ is viscous work term, $U \cdot S_M$ is work due to external momentum sources which are neglected and S_E is the energy source.

These equations are discretized to algebraic equations and then numerically solved with ANSYS CFD which is based on the Finite Volume technique.

B.2   Grid

Before discussing the grid decision, some terms have to be defined.

B.2.1   Wall function and Y-plus

Boundary conditions have to be settled before solving governing model equations. Flow conditions near to no-slip walls are calculated by using wall functions. These functions assume the velocity distribution near the wall (see figure B.1) can be described as a logarithmic profile. The fluid shear stress function is depending on the fluid velocity at a given distance from the wall, known as the *log law of the wall*. Near the wall the velocity, U, and wall shear stress, τ_ω, will pose a problem. Theory and experiments shows that the boundary layer consists of two layers; closest to the wall lays the viscous layer and here the velocities have greatest influence. In the logarithmic layer the mixing turbulence is the dominating variable. Between these to layers is a region called the buffer layer, and here both viscosity and turbulent have equal influence.

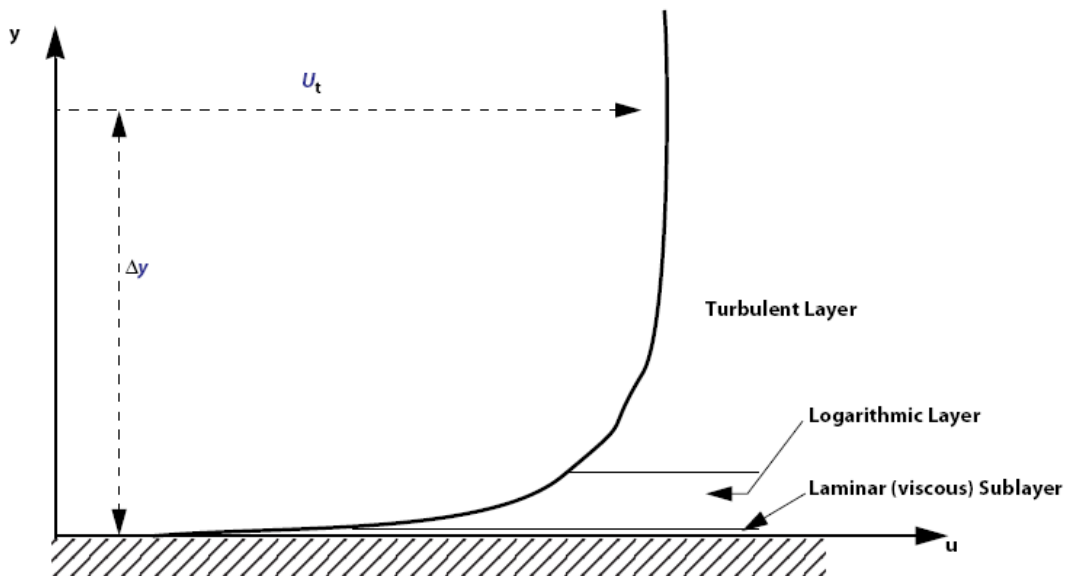

Figure B.1: Near wall region [3]

A scalable wall-function(Equation B.4) determines the near wall conditions by scaling the variables. The velocity profile can be predicted while it change from linear to logarithmic

behaviour with increasing Reynolds number.

Y-plus is a dimensionless factor that defines the distance between the wall and the first grid element. In the first elements near the wall, y-plus values within 20 and 300 are accepted while the numerical error will be small. The wall function is related to wall shear stress, u_τ [18] :

$$u^+ = \frac{U_t}{u_\tau} = \frac{1}{\kappa}\ln(y^+) + C \tag{B.4}$$

where y^+ and u_τ is defined below

$$y^+ = \frac{\rho\Delta y u_\tau}{\mu} \tag{B.5}$$

$$u_\tau = (\frac{\tau_\omega}{\rho})^{1/2} \tag{B.6}$$

where

- u^+, near wall velocity

- u_τ, friction velocity

- U_t, known velocity tangent to the wall at a distance of Δy from the wall

- y^+, dimensionless distance from the wall

- τ_ω, wall shear stress

- κ, von Karman constant

- C, log-layer constant depending on the wall roughness

B.2.2   Turbulence models

The two most common turbulence models are the k-ϵ and Shear Stress Transport (SST). The k-ϵ model is often used by the industry because it is numerically robust, while it also is computational accurate. The k-ϵ model has its limitations with rotating fluids, curved surfaces and separation predictions. SST calculates the conditions near the wall by blending k-ϵ and k-ω model. In the k-ω model the treatment of low Reynolds number are more accurate and robust, and it requires a y+ $\leq$ 2 and at least 15 nodes in the boundary layer near the wall to avoid numerical errors. When introducing particles in the domain, the treatment near the wall is important and no loss of data is desirable. Therefore a SST model is preferable since it gives a more accurate prediction of the flow in these areas.

B.3 Particle Transport model

Ansys CFX Particle Transport model is a numerical study to predict where particles collide with the wall, also known as impact zones of erosion. Including sand in the system, the water will be handled as a multiphase flow where the sand particles are a dispersed phase. The Langrangian Tracking model is used to track the particles through the flow.

Even though the particles have a specified diameter they are modelled as moving points and will not take up volume from the fluid, and particle-particle interactions are neglected.

B.3.1 Erosion

Erosion is a result of particle momentum change, which lead to a force on the wall. The erosion rate density corresponds to shear stress and pressure from the flow. In the simulations erosion of a wall due to one particle is calculated by[3]:

$$ErosionRate = E * N * m_p \tag{B.7}$$

where E is representing an individual particle, m_p is the mass of the particle and N is the actual number of particles the one particle represents. The total erosion is a summation of all the particles injected. In the results, the erosion rate density is given as $kg/m^2 s$ and is a qualitative guide to erosion. The Finnie model is weak for angles at 90 degrees and to cope with this a user-defined Fortran code can be implemented. This is not done in this project.

B.3.2 Forces acting on the particles

Viscous drag will influence the fluid to change velocity and direction of the particles. At the same time, also particles can have an effect on the fluid flow. In the CFD simulation, this effect is called phase coupling. *The Fully Coupled* set of particles allows the particles to influence the continuous flow. *One-way Coupled* particles only follow the flow field. By making two different sets of particles, a more accurate calculation of the particle volume fraction and local forces on the wall are rendered.

In the intermediary region between the viscous and inertial area, spherical particles will be affected by both the viscous and inertial forces. To take into count these effects Schiller and Naumann determined the drag coefficient as a function of Reynolds number [3]. For simulations with solid particles, the drag forces are best handled with the *Schiller Naumann Drag Model*.

$$C_D = \frac{24}{Re}(1 + 0.15Re^{0.687}) \tag{B.8}$$

Forces of gravity also have influence on the particle, but since other forces like drag and inertial forces are larger, the buoyancy force can be neglected.

For rotating fluid machinery models, it is useful to specify the domain as a *rotating frame of reference*. The angular velocity, ω, is 600 rpm and the direction is decided by the right-hand rule, and then Coriolis and centrifugal momentum terms are calculated [3].

B.4 Elements of Error and Uncertainty

Errors and uncertainty are important parts of the CFD calculations and have to be considered. [18]

Numerical errors involve miscalculation in the analysis like round off error, iterative convergence error and discretisation error. Verification of a model involves error quantification by comparing CFD results with predicted results. A plot of e.g. pressure distribution and velocity vectors can be of use to determine errors.

Uncertainties are associated with input values such as domain geometry, boundary conditions and fluid properties. Validation of a model involves quantification of input uncertainties. For example, a test on the model for different input data can give an analysis of the sensitivity in the model.

The best validation for CFD analysis is to compare with experimental data.